PHILOSOPHICAL TRANSACTIONS OF THE ROYAL SOCIETY A MATHEMATICAL, PHYSICAL & ENGINEERING SCIENCES

The Constitution of Alloys of Iron and Manganese with Transition Elements of the First Long Period

A. Hellawell and W. Hume-Rothery

Phil. Trans. R. Soc. Lond. A 1957 **249**, 417-459
doi: 10.1098/rsta.1957.0004

THE CONSTITUTION OF ALLOYS OF IRON AND MANGANESE WITH TRANSITION ELEMENTS OF THE FIRST LONG PERIOD

By A. HELLAWELL and W. HUME-ROTHERY, F.R.S.

Department of Metallurgy, University of Oxford

(*Received* 8 *June* 1956—*Revised* 18 *July* 1956)

CONTENTS

	PAGE
1. Introduction	418
2. Experimental	418
(*a*) Metals used	418
(*b*) Furnace construction	419
(*c*) Refractory materials	420
(*d*) Thermocouples	420
(*e*) Experimental procedure	421
(*f*) Microscopical and X-ray examination of ingots	422
(*g*) Analysis of the ingots	422
(*h*) Annealing technique	422
3. Thermal arrests and accuracy of results	422
(*a*) Thermocouple–e.m.f. relations	423
(*b*) Identification of liquidus-curve arrests	423
(*c*) Identification and accuracy of solidus-point arrests	424
(*d*) Accuracy of arrest points for transformations in the solid state	426
4. Experimental results for iron alloys	427
(*a*) Pure 'H' iron	427
(*b*) Iron–titanium	427
(*c*) Iron–vanadium	429
(*d*) Iron–chromium	429
(*e*) Iron–manganese (iron-rich alloys)	430
(*f*) Iron–nickel	431
(*g*) Iron–cobalt	432
(*h*) Iron–copper	432
5. Experimental results for manganese alloys	433
(*a*) General	433
(*b*) Pure manganese	433
(*c*) Manganese–titanium	434
(*d*) Manganese–vanadium	434
(*e*) Manganese–chromium	436
(*f*) Manganese–iron	438
(*g*) Manganese–cobalt	439
(*h*) Manganese–nickel	441
(*i*) Manganese–copper	441
5. Discussion	442
(i) The equilibrium diagrams of iron and manganese alloys	442
(ii) Relative depressions of liquidus and solidus curves for solid solutions in δ- and γ-Fe	445
(iii) Relative depressions of liquidus and solidus curves for solid solutions in δ- and γ-Mn	447
(iv) Van't Hoff's equation and the latent heats of fusion of δ-Fe and δ-Mn	449
(v) Further examination of the δ/γ/liquid equilibrium	450
(vi) The γ/δ/liquid equilibrium	452
Appendix A. Results of thermal analysis	453
Appendix B. Chemical analysis	457
References	459

Using metals of the highest purity, the constitutions of iron-rich and manganese-rich binary alloys with the sequence of elements Ti–V–Cr–(Mn, Fe)–Co–Ni–Cu have been investigated by specially accurate thermal analysis, supplemented by microscopical and X-ray work. The liquidus and solidus curves have been determined accurately, and also the forms of the A_4 (γ/δ) transformations in the iron alloys, and of the (γ/δ) and (γ/β) transformations in the manganese alloys. The complete liquidus and solidus were determined for the system Fe–Mn, and the equilibrium diagrams of the systems Fe–Ti and Mn–Ti were studied as far as 52 at. % Ti.

Vol. 249. A. 968. (Price 13*s*. 6*d*.) 51 [Published 14 March 1957

δ-Mn (b.c.c.) and γ-Mn (f.c.c.) have the same crystal structures as δ-Fe and γ-Fe respectively, and the corresponding parts of the equilibrium diagrams are thus structurally comparable. In general, there is a remarkable correspondence between the effects of the different elements in stabilizing the b.c.c. or f.c.c. phases. The closed γ-loops in the systems Fe–Ti, Fe–V and Fe–Cr are paralleled by closed γ-fields in the Mn alloys, whilst Mn (in Fe), Fe (in Mn) and Ni produce open or expanded γ-fields; Cu behaves abnormally in both series of alloys. In the Mn alloys, the stability and range of the β-Mn phase reach a maximum in the system Mn–Co, where the β-Mn phase is so stable that it comes into equilibrium with the liquid, and prevents the formation of a continuous series of solid solutions between γ-Mn and β-Co (f.c.c.).

For the iron alloys the size factors are favourable for all the solutes examined, except Ti, which lies on the borderline of the favourable zone. With δ-Mn and γ-Mn as solvents, the size factors are all favourable, although that for Ti is still appreciable (*ca.* 10 %). The effect of size factor is shown by steep depression of the δ-liquidus and δ-solidus curves in the systems Fe–Ti and Mn–Ti. For the iron alloys the relative depressions of liquidus and solidus at equal atomic percentages of solute are in the order Ti > V > Cr and Co < Ni < Cu, and these sequences are the same as those for the lattice distortions produced by equiatomic percentages of the same solutes; the effect of Mn lies out of sequence in both cases. These and other relations are discussed.

When compared with previous diagrams, the general effect of the present work is to indicate a much narrower two-phase (liquid and solid) range for both δ-Fe and γ-Fe solid solutions. In marked contrast to previous diagrams, the present liquidus and solidus curves can all be reconciled with the existence of monatomic solutions in both liquid and solid phases. For Fe–Mn alloys the equations for dilute solutions are in good agreement with thermal data for pure iron up to 30 at. % Mn.

1. Introduction

The metal iron is unique in possessing body-centred cubic structures at high (δ-iron) and low (α-iron) temperatures, with the face-centred cubic γ-iron as the stable form in the temperature range 910° to 1390° C. Recent work by Basinski & Christian (1954) has shown that of the four allotropic forms of manganese, the high-temperature forms γ-manganese and δ-manganese have f.c.c. and b.c.c. structures respectively, so that with falling temperature the sequence liquid → b.c.c. → f.c.c. is the same in both metals. It was thus of interest to compare the high-temperature portions of the equilibrium diagrams of alloys of iron and manganese with the transition elements of the first long period. The present paper describes an investigation of the constitution of iron-rich and manganese-rich alloys with the elements titanium, vanadium, chromium (manganese–iron), nickel and copper, and of the system manganese–cobalt. This work, together with that of Harris & Hume-Rothery (1953) on the system iron–cobalt, enables the whole of the two series of alloys to be compared. In the system iron–manganese the complete liquidus and solidus curves have been established. Nearly all of the present work has been carried out by methods of thermal analysis; the experimental details are described in § 2, and the accuracy and reproducibility of the results are discussed in § 3. Sections 4 and 5 describe the experimental results for the iron alloys and manganese alloys respectively, and in § 6 the equilibrium diagrams are compared and discussed.

2. Experimental

(*a*) *Metals used*

The iron used in the present work was kindly presented by the British Iron and Steel Research Association, and was 'H' iron of approximately 99·95 % purity. The freezing-point was determined as 1533° C, with an A_4 (δ/γ) transition temperature of 1389° C. The

accepted values for iron of the highest possible purity are 1534 and 1388° C respectively.* The manganese used was high-purity electrolytic metal from Johnson, Matthey and Co. Ltd. The first batches were given a high-temperature treatment with hydrogen, but this practice was discontinued when, as described in § 5, it was found that the freezing-points of manganese alloys as determined in hydrogen were lower than those determined in argon. The details of the remaining metals are given in §§ 4 and 5.

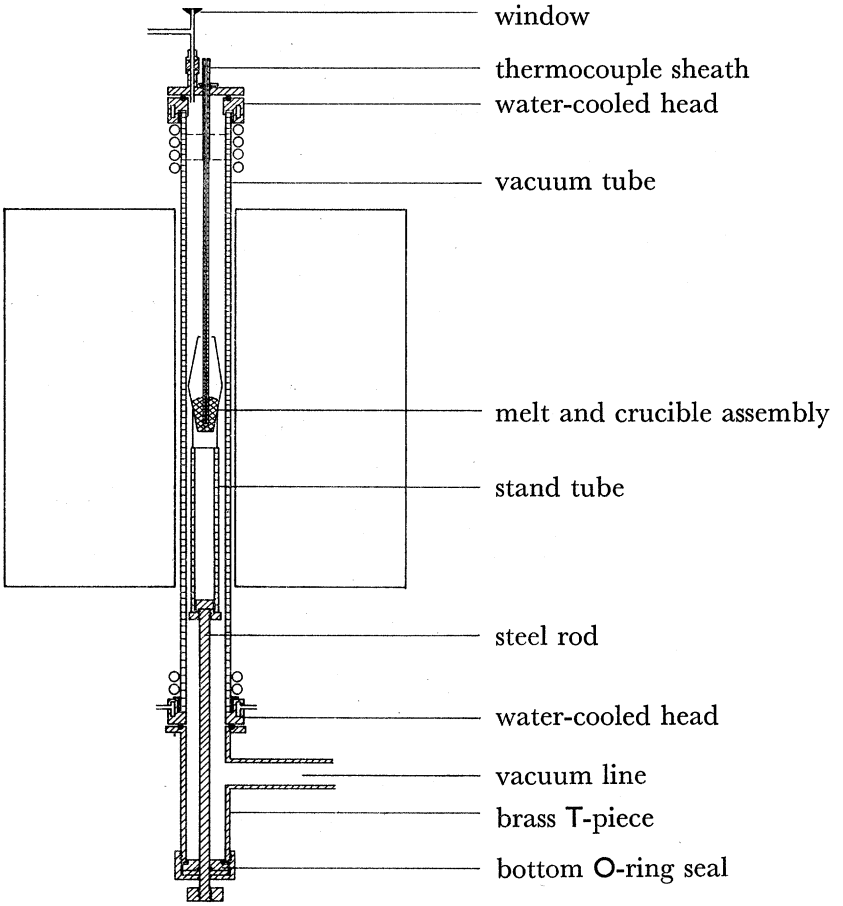

FIGURE 1. Section of apparatus.

(*b*) *Furnace construction*

The heating curves and cooling curves were taken with the specimen in a closed refractory tube, with water-cooled heads, which was either continuously evacuated, or filled with an inert gas. For convenience we refer to this as the vacuum tube, to distinguish it from the tube of the furnace. The vacuum tube passed through a vertical, platinum-wound, resistance furnace whose current was controlled by a Variac transformer. The apparatus was based on that of Harris & Hume-Rothery (1953) and is shown in figure 1. The main characteristic of this is that the crucible containing the alloy can be raised into, or lowered from, the hot part of the vacuum tube without breaking the vacuum system. For convenience in manipulation the top head of the tube was redesigned.

* This value (1388° C) is that of Adcock (1937) and is quoted by *A.S.M. Handbook* 1948 as the most accurate value. The value of 1400° C reproduced in many diagrams appears to be taken from earlier and less accurate work.

The vacuum tubes were evacuated through the bottom head by means of $1\frac{1}{4}$ in. diameter brass tubing leading directly to an Edwards 102 diffusion pump, using silicone oil, and backed by a single- or double-stage rotary pump. Pressures were measured by Penning-type gauges supplied by Edwards and Co. Ltd, and tests were made to ensure that the pressure at the top head of the furnace was essentially the same as that above the pump. Carefully purified hydrogen or argon could be admitted to the vacuum tube through the top head.

During the course of the work a battery of three furnaces was made, each with its own vacuum system, but with a common gas system which by means of taps could be made to serve any desired furnace. One of the furnaces was used exclusively for checking thermocouples against the freezing-point of pure nickel; owing to the volatility of manganese, the alloys of this element were confined to one furnace.

(*c*) *Refractory materials*

For temperatures above 1500° C, use was made of recrystallized alumina vacuum tubes supplied by the Morgan Crucible Co. Ltd; these had a long life and good resistance to thermal shock. For some of the work at lower temperatures Morgan 'mullite' tubes were used, and although these were satisfactorily vacuum-tight, they tended to crack when the hot crucible assembly was lowered into the cold part of the vacuum tube.

The crucibles used were made of Morgan's recrystallized alumina and appeared to be unattacked by all the alloys except those containing high percentages of titanium which are referred to in §§ 4 and 5. The weight of the cooling curve ingots was of the order 30 to 50 g, and the melt crucible was contained inside a larger crucible (figure 1) which provided a firm support and retained the molten metal in the event of fracture of the melt crucible. A second crucible fitted as a lid served to reduce volatilization of metal and also to lower the temperature gradients in the melt.

The thermocouple sheaths were obtained from Degussa, Department Degussit, Frankfurt, Germany, and were vacuum-tight 'Degussa' alumina tubes of 3·5 mm external and 2 mm internal diameter, 40 cm long.

(*d*) *Thermocouples*

Temperatures were measured by means of Pt/Pt–Rh thermocouples in conjunction with a Carpenter–Stansfield potentiometer and Cambridge galvanometer. The wires were of 0·015 in. diameter, and two kinds of thermocouple were used. One of these was of the standard Pt/Pt 13 % Rh type, and was used in connexion with the e.m.f.-temperature tables of the British Standards Institution. These thermocouples were repeatedly calibrated against the freezing-point of nickel which was taken to be 1453° C, and it was assumed (see p. 423) that in the range 1350 to 1540° C a constant correction could be applied equal to the difference between the observed and standard values of the e.m.f. at the nickel point. The second batch of thermocouples was of the Pt 2 % Rh/Pt 13 % Rh type, the former wire being made specially by Johnson, Matthey and Co. Ltd. A standard e.m.f.-temperature curve for this series was determined by the late Mr G. B. Harris from observations of the freezing-points of zinc, silver, gold, nickel and palladium. In the present work check calibrations were again made repeatedly against the nickel point (1453° C), and for some of the lower temperatures the freezing-point of the high-purity

manganese (1244° C) was used as a secondary calibration point. Experience showed that if thermocouples were heated below 1300° C their changes were negligible, but that when heated to between 1500 and 1600° C their behaviour was unpredictable, and that whereas one thermocouple might show changes of less than 1° C after 10 to 12 experiments at 1500° C, another might show changes of 2 or 3° C after two or three cooling curves. It was thus necessary to avoid exposing the thermocouples to a high temperature for longer than was essential, and it was found advisable to use one thermocouple for the approximate control of the temperature during the melting process and preliminary cooling (or annealing treatment), and to replace this by a second thermocouple for the exact measurement of the arrest points, the second thermocouple being used for the shortest possible time.

(*e*) *Experimental procedure*

In a typical experiment the vacuum tube assembly would be thoroughly degassed overnight with the alloy in the cold part of the tube, and the furnace at about 900° C. The crucible assembly was then slowly raised into the hot zone, and for the iron alloys the pressure was not allowed to exceed 2×10^{-4} mm Hg. For the manganese alloys a pressure up to 10^{-3} mm Hg was tolerated because of the considerable evolution of hydrogen which always occurs when this metal is heated. For the nickel-point calibrations, and for the alloys of iron with chromium or nickel, the constituent metals were heated *in vacuo* until completely molten, and were then treated with hydrogen, which was slowly pumped off before carrying out the thermal analysis *in vacuo*. For the alloys of iron, with titanium and vanadium, the treatment with hydrogen was not possible, and the whole operation was carried out *in vacuo*, with extreme precautions to prevent a rise in pressure above 10^{-4} mm Hg. For the alloys of iron with the relatively volatile metals manganese and copper, the melting process and thermal analyses were carried out in argon, whilst for the manganese-rich alloys, experiments were carried out in both argon and hydrogen, and these details are described in § 5.

The constituent metals, or the pre-melted alloy (details are given in §§ 4 and 5), were heated until completely molten and, after thorough stirring of the melt, the Variac transformer was set so as to give a rate of cooling of about 2 to 3° C/min at the expected arrest point. Stirring was effected by the thermocouple sheath. The upper end of the sheath was sealed with black wax into a short length of glass tubing, which made an efficient sliding vacuum seal through a well greased 'O' ring in the top head of the furnace. The actual opening in the lid of the furnace was sufficiently large to permit the tip of the sheath to be moved from side to side within the furnace. The alloy was stirred during the taking of the cooling curve, and as soon as the arrest was established the adjustments of the galvanometer and potentiometer circuits were checked, and the uniformity of temperature throughout the ingot was tested by raising and lowering the thermocouple. For the iron alloys the cooling curve was continued until the solidus point was passed and the alloy was then held slightly below this point for about 30 min, after which the cooling curve was continued, and followed by a heating curve until the alloy* was completely liquid. For the manganese alloys, a similar procedure was followed.

* In some alloys very near to the δ/γ peritectic it was not possible to hold the alloy in the temperature region of the δ-field, and the alloy was annealed at a lower temperature.

PHILOSOPHICAL TRANSACTIONS OF THE ROYAL SOCIETY A MATHEMATICAL, PHYSICAL & ENGINEERING SCIENCES

(*f*) *Microscopical and X-ray examination of ingots*

The ingots of the iron alloys* were sectioned longitudinally, and a count of oxide particles was made as in the work of Harris & Hume-Rothery (1953). It was found that the presence of 0·01 % of oxygen corresponded to a count of approximately 200 oxide particles in a longitudinal traverse, and in most systems a typical ingot was analyzed by vacuum fusion methods. The results suggested that oxidation during the thermal analysis was small, and the probable oxygen content of a typical ingot was of the order 0·005 % as compared with a value of 0·003 % for the 'H' iron. The microscopical examination was also useful in confirming the forms of some of the equilibrium diagrams. The manganese alloys were, in general, too brittle for examination in this way, but a little microscopical work was carried out. A few X-ray diffraction experiments were also made, both on powder prepared from the ingots, and from the flat sections, and the results are referred to in § 5 for the systems Mn–Ti and Mn–Co. Standard methods were used for the annealing and quenching experiments below 1200° C.

(*g*) *Analysis of the ingots*

After microscopical examination, the complete cooling curve ingots, or half ingots, were dissolved for chemical analysis. This work was carried out by the B.I.S.R.A. Research Laboratory at Sheffield, and we have to express our extreme gratitude to Mr K. Speight for his care and attention (see appendix B). After preliminary work had shown that no appreciable contamination occurred,† the general practice was to determine the solute element only, because the methods available for the determination of iron are not sufficiently precise for the exact totals of the analytical percentages of the two metals to be significant. Numerous spectrographic analyses were also carried out, and confirmed the purity of the alloys except for the small amounts of tungsten referred to in § 4. The analytical methods used are summarized in appendix B, from which it will be seen that, so far as the analytical methods are concerned, the composition should be accurate (see appendix B) to within $\pm 0{\cdot}1$ %. Where half ingots were analyzed, the possibility of uneven composition introduces a further slight error.

(*h*) *Annealing technique*

Standard methods were employed for annealing. Alloys were sealed off *in vacuo* or under argon within silica capsules. Furnaces were controlled to within $\pm 1{\cdot}5°$ C up to 1250° C and specimens were quenched into iced water.

3. Thermal arrests and accuracy of results

The accuracy of the present results depends on (*a*) the accuracy with which the temperature–e.m.f. relations of the thermocouples was known, and (*b*) the accuracy with which the true arrest points could be deduced from the thermal curves.

* The iron–titanium alloys could not be examined in this way.

† As explained later, slight contamination by tungsten was found in some of the arc-melted alloys.

(*a*) *Thermocouple–e.m.f. relations*

All the present data are referred to the nickel point, which is taken to be 1453° C. Our experiments suggest that, under strictly standardized furnace conditions, the nickel point is reproducible to within ±0·5° C. The assumption of a constant correction (based on the nickel point) for the range 1350 to 1540° C should not have introduced errors greater than ±1° C, and detailed examination suggested that the use of the Pt 2 % Rh/Pt 13 % Rh thermocouple instead of the standard Pt/Pt 13 % Rh should not have introduced errors greater than 0·5° C. So far as the temperature–e.m.f. relations are concerned, the accuracy of the present temperature readings relative to the nickel point of 1453° C should be of the order ±1 to ±2° C, and the accuracy should increase slightly in the immediate region of the nickel point. If the present results are expressed in degrees Kelvin, it must be remembered that the nickel-point value (1453+273=1726° K) is itself uncertain by a few degrees.

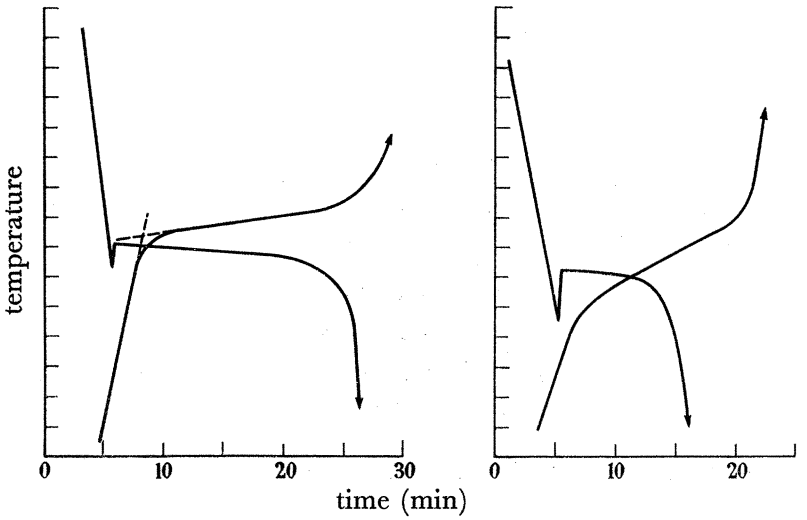

FIGURE 2. Pure nickel. FIGURE 3. Pure iron.

FIGURES 2 AND 3. Thermal arrests on freezing and melting. (Temperature scale in 1° C intervals.)

(*b*) *Identification of liquidus-curve arrests*

The liquidus points were determined from the results of cooling curves alone. In the diagrams the points are represented ▽, and the lower apex of the triangle is the recorded temperature. In general, the arrests showed a slight supercooling, and sometimes very slight rounding of the curves in the region of the arrest. The arrests on heating curves showed a similar but more pronounced rounding, and in both cases the policy adopted was to extrapolate the curve as shown by the dashed lines in figure 2. Figure 2 shows a cooling curve and heating curve for pure nickel, and for this the freezing range is narrow (*ca.* 1° C), and the extrapolated intersections for the beginnings of the arrests on the two curves agree within 0·5° C. The extrapolated value for the end-point of the heating curve arrest is ~1·5° C above the value for the beginning of the arrest. Figure 3 shows similar curves for the 'H' iron, and the change takes place over a slight range of temperature. The extrapolated intersection for the beginning of the arrest on the heating curve is about

1·0° C below, and that for the end of the arrest is about 1·5° C above, the value for the cooling curve. With alloys showing well-defined arrests, the beginning of the cooling-curve arrest could be identified with roughly the same degree of accuracy. Of the alloys examined, the liquidus curve fell most steeply in the system iron–titanium, and experiments were carried out at different rates of cooling for an alloy containing 19 % of titanium, for which the liquidus curve is falling very steeply. The results for this alloy are shown in figure 4, and it will be seen that an increase in the rate of cooling from 1·5 to 5° C/min lowered the liquidus arrest by only 1° C.

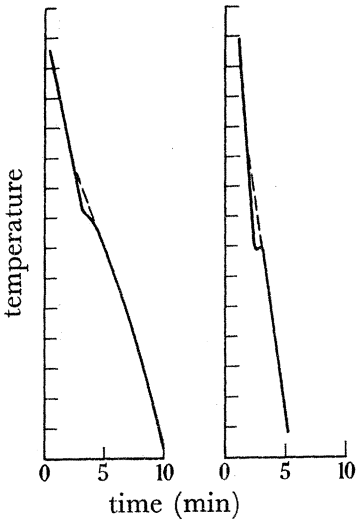

(*a*) 2° C/min. (*b*) 5° C/min.

FIGURE 4. Liquidus arrests for different rates of cooling; Fe—19 at. % Ti. (Temperature scale in 1° C intervals.)

It is reasonable to conclude that the identification of the exact liquidus arrest point on the cooling curves may introduce errors increasing from ±0·5° C for iron-rich alloys to ±1° C in less favourable cases. To these errors must be added those resulting from temperature gradients within the melt, since these could not be guaranteed to be less than ±1° C, although the recorded gradients were often within ±0·5° C. Apart from these errors in taking or interpreting the thermal curves, there are the thermocouple errors referred to previously which, relative to a nickel point of 1453° C, should not exceed 1·5° C in the range 1350 to 1540° C, but may be as much as ±2° C outside this region, although a check against the gold point showed that the assumption of a constant correction involved an error of less than 1° C.

If smoothed curves are drawn through the observed liquidus points to pass through the observed freezing-points of the 'H' iron (1533° C) and manganese (1244° C), it is reasonable to claim that the liquidus curves of the iron-rich and manganese-rich alloys may be discussed or compared to an accuracy of ±2° C.

(*c*) *Identification and accuracy of solidus-point arrests*

The solidus points were determined from the beginnings of the arrests on heating curves, and are represented △, the upper apex of the triangle giving the recorded temperature. The solidus arrests on the heating curves of alloys were always more rounded

than the liquidus arrests on cooling curves, and the extrapolation method was again used (see figures 2 and 3). With some alloys, the time of annealing in the solid state was increased from $\frac{1}{2}$ to 2 h, but there was no improvement in the sharpness of the arrest, and no appreciable change in the extrapolated arrest point. This shows that any effect of uneven composition is not due to a short-range cored structure. Much of the rounding off of the cooling curves is probably due to slight temperature gradients in the specimens, but for some alloys the effect was greater.

For the iron-rich alloys, the identification of the exact solidus arrest point should not have introduced errors greater than $\pm 2°$ C, to which must be added the thermocouple errors described above. The tables and diagrams give the observed results, but as explained

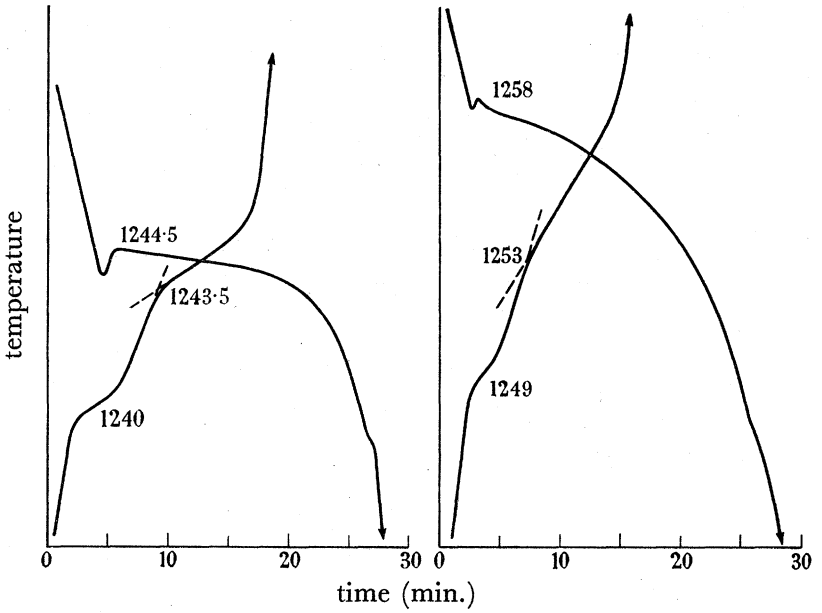

(*a*) pure Mn. (*b*) Mn—3·0 % at % V.

FIGURE 5. Liquidus and solidus arrests for pure manganese and for an alloy.

above the arrest on the heating curve of the 'H' iron was about 1° C lower than the beginning of the arrest on the cooling curve, and it is probable that solidus points for most iron-rich alloys are low by an amount of this order.

For the manganese alloys, curious results were obtained which could not be understood. Figure 5*a* shows a cooling curve for pure manganese. The freezing-point arrest is almost horizontal and indicates a freezing-point of 1244·5° C. The heating curve shows a well-defined arrest at 1240° C, of which there is a very faint sign on the cooling curve,* and this is followed by an arrest extending from 1243·5 to 1245° C which clearly corresponds to the first arrest on the cooling curve. Figure 5*b* shows the effect for a manganese–vanadium alloy. The difference between the two arrests was about 3° to 4° C in all the alloys, and this makes it most improbable that the effect is due to the existence of a fifth allotropic modification of manganese above δ-manganese. In spite of much work, the cause of the effect could not be established, and the temperatures recorded in the tables are those of the higher arrests to correspond with the solidus. The ignoring of the lower arrest may be

* The arrest is inevitably slight because it occurs at the steeply falling part of the curve.

criticized, but the only alternative appeared to be to give a diagram in which 'pure' manganese freezes over a range of 3 to 4° C.

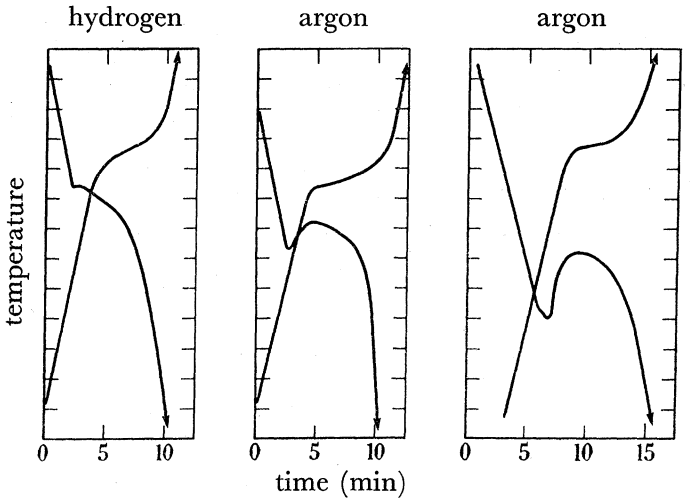

(*a*) γ/δ. (*b*) γ/δ. (*c*) β/γ.

FIGURE 6. Observed solid-state arrests in pure manganese. (Temperature scale in 1° C intervals.)

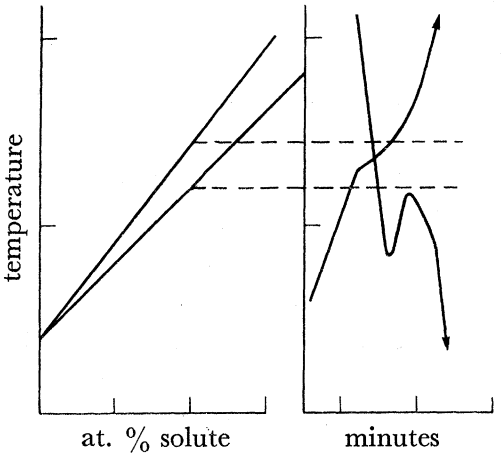

(*a*) actual phase diagram. (*b*) observed arrests.

FIGURE 7. Hysteresis in solid-state arrests.

(*d*) *Accuracy of arrest points for transformations in the solid state*

Owing to the existence of temperature hysteresis, the use of thermal analysis for the investigation of transformations in the solid state is less accurate than for the liquidus and solidus curves. In the iron alloys with expanded or open γ-fields, the two-phase $(\gamma+\delta)$ region is narrow. Its width at the peritectic temperature is determined fairly accurately by the intersections of the solidus curves with the peritectic horizontals. In the absence of hysteresis the cooling curve should give an arrest corresponding to the $\delta/(\delta+\gamma)$ boundary, and the heating curve should give an arrest at a *lower* temperature, corresponding to the $\gamma/(\delta+\gamma)$ boundary. This behaviour was shown by alloys whose δ/γ transformation temperatures were near to those of the peritectic horizontals, although detailed examination

showed a tendency for the cooling-curve arrest to be slightly lower, and the heating-curve arrest to be slightly higher than indicated by the composition at the peritectic. At lower temperatures, the two-phase region becomes very narrow, and there was a tendency for the heating-curve arrests to be a few degrees *higher* than the cooling-curve arrests. In such cases the policy adopted is to draw a single line in the diagram to represent the region of the δ/γ change, but it must be emphasized that this is not an accurate determination, and that a narrow two-phase region undoubtedly exists (see figure 7).

4. Experimental results for iron alloys

For convenience the results of the thermal analyses are summarized in tables A1 to A7, appendix A. All compositions are in atomic percentages of the solute elements concerned. For abbreviation chemical symbols are often used in the text, and alloys are referred to in terms of their atomic percentages so that, in a system Fe–X, alloy 24·5 means an alloy containing 24·5 atomic per cent (at. %) of X. The relation between the present result and those of previous investigations is indicated briefly, but for reasons of space it has not been possible to publish any detailed comparison or to reproduce more than a very few of the earlier diagrams.

(*a*) *Pure* 'H' *iron*

The freezing-point of the 'H' iron was determined as 1533° C, in agreement with the work of Harris & Hume-Rothery (1953), and with the value 1534° C obtained by Schofield (1954, private communication) for metal of comparable purity. As explained on p. 423 the freezing process always took place over a slight range of temperature. The A_4 (δ/γ) transition point was determined as 1389° C, the values from cooling and heating curves being 1388 and 1389·5° C respectively.

(*b*) *The system iron–titanium*

The results of the thermal analyses are shown in table A1, and are plotted in figure 8. Alumina crucibles were found satisfactory for alloys containing up to 30 at. % Ti, but beyond this point rapid attack of these crucibles took place, and quite spurious results were obtained (see p. 428). By the use of thoria crucibles (made by the Morgan Crucible Co. Ltd) and thoria-coated thermocouple sheaths the work was extended to 50 at. % Ti without contamination from the refractories. The majority of the alloys were pre-melted in an argon-arc furnace (see table A1), and very small amounts of tungsten were introduced in this way. Except for alloy 1·29 the proportions of tungsten was of the order $<0{\cdot}01$ at. % and should have no appreciable effect on the liquidus and solidus.*

From figure 8*a* it will be seen that the addition of titanium produces a rapid fall in the liquidus and solidus curves of δ-iron which fall to a eutectic horizontal at 1289° C, corresponding to the reaction:

$$\text{liquid } (16) \rightleftharpoons \text{solid } \delta\ (9{\cdot}8) + Fe_2\,Ti.$$

The solidus arrests in the range 5 to 10 at. % Ti were the most difficult of the series to locate exactly, and for these the accuracy is estimated as being of the order $\pm 5°$ C. From the eutectic point the liquidus rises to a rather flat maximum at 1427° C, the melting-point

* The depression of the liquidus curve is of the order 0·2° C for 1 at. % W.

of the compound Fe_2Ti, and then falls to 1317° C, at which temperature the compound FeTi is formed by a peritectic reaction.

When alloys in the range 30 to 50 at. % Ti were melted in alumina crucibles, the liquidus continued to rise with increasing titanium content, presumably owing to the formation of ternary (Fe–Ti–Al) or quaternary (Fe–Ti–Al–O) alloys. This effect was very

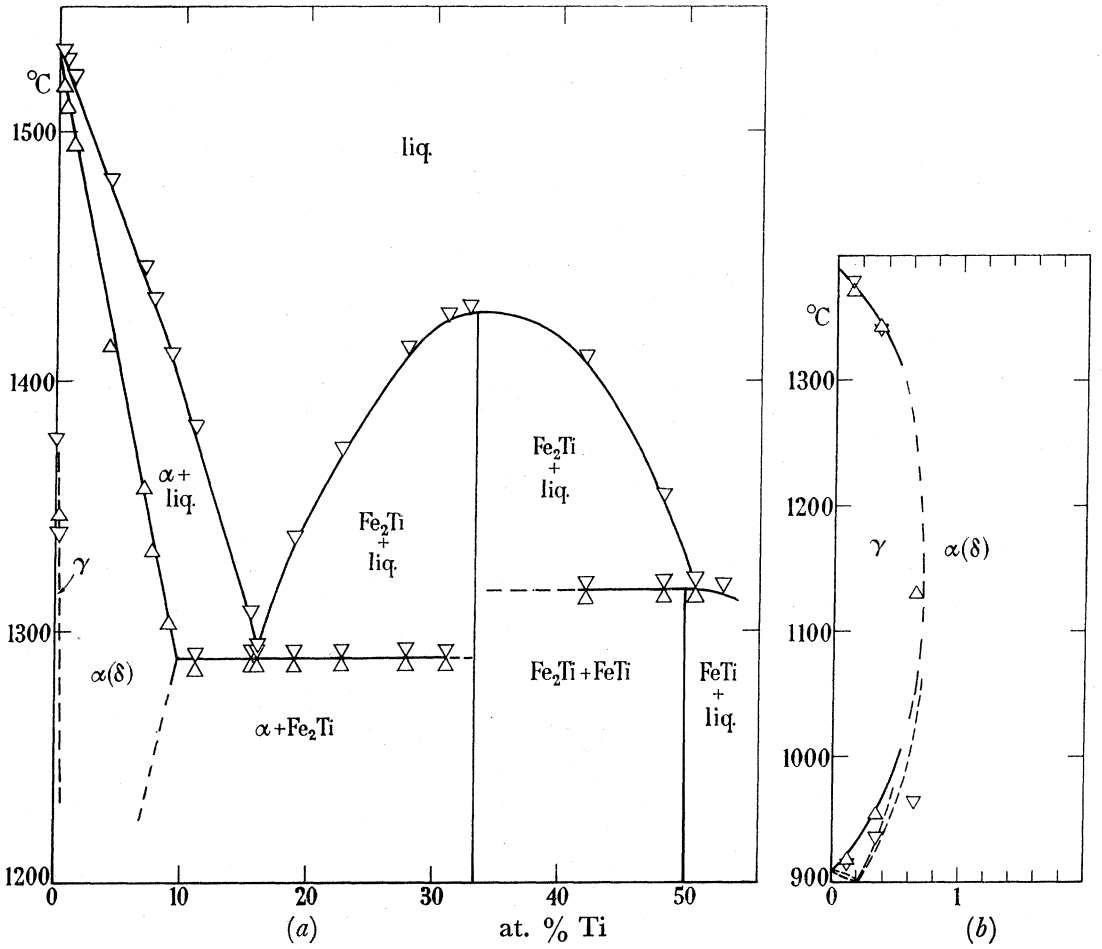

FIGURE 8. (*a*) Phase diagram for Fe–Ti above 1250° C from 0 to 52 at. % Ti. (*b*) Fe–Ti γ-loop showing thermal arrests obtained in present work. (Dashed lines show diagram after Fishel and co-workers.)

marked, and at 50 at. % Ti the liquidus arrests for contaminated alloys were as much as 150 to 200° C higher than those shown in figure 8, and contamination of this kind is probably responsible for some of the discrepancies between the diagrams of previous investigators.

The form of the present diagram confirms previous work in the range 0 to 30 at. % Ti, but places the eutectic temperature (1289° C) appreciably lower than the value (1310° C) given by Witte & Wallbaum (1938), whilst the melting-point of the compound Fe_2Ti (1427° C) is also much lower than the previous value (1530° C). From 30 to 50 at. % Ti the present results disprove the diagrams of Witte & Wallbaum (1938), but confirm the general type of diagram proposed by American workers (see Hansen, McPherson & Rostoker 1953 for a summary of the data on this system), although the exact temperatures

were previously uncertain. The existence of a γ-loop without a minimum is suggested by the thermal arrests for alloys 0·11, 0·36 and 0·63, but temperature hysteresis prevents these from being accurate (figure 8*b*).

(*c*) *The system iron–vanadium*

The results of the thermal analyses are shown in table A2 and figure 9. The vanadium used was supplied by Johnson, Matthey and Co. Ltd, and was in the form of beads of 99·8 % purity, the chief impurity being iron. Alloys 0·54 and 1·55 were prepared by the direct melting of the constituent metals, and all other alloys were pre-melted in an argon-arc furnace. The close agreement between the results for alloy 10·5 containing 0·2 at. % W

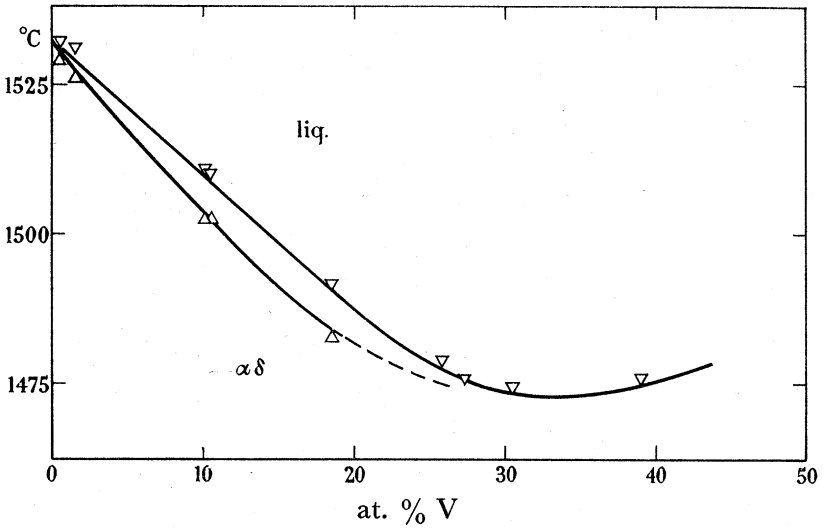

FIGURE 9. Liquidus and solidus curves for Fe–V, from 0 to 30 at. % V.

and 10·1 containing 0·05 at. % W suggests that no appreciable effect was produced by the slight contamination of these two alloys. Owing to the restricted amount of vanadium available, it was necessary to reduce the weight of the cooling-curve ingots to 15 g, and smaller narrower crucibles were used in order to ensure good immersion of the thermo-couple. The equilibrium diagram of the system Fe–V (Smithells 1955) is of the γ-loop type, with a continuous range of solid solutions between the b.c.c. vanadium, and the $\alpha\delta$-iron. The liquidus passes through a minimum at about 33 at. % V, and at lower temperatures a σ-phase is formed from the α-solid solutions. For alloys containing more than 20 % V the solidus arrests were unsatisfactory and have therefore been omitted.

The present liquidus and solidus curves fall smoothly up to 20 at. % V, and indicate a much narrower freezing range than that of the previously accepted diagram. The arrests at higher percentages of vanadium confirm the existence of a minimum in the liquidus and solidus curves in the region of 33 at. % V, but the exact composition was not determined. The low-temperature arrests for alloy 0·54 confirmed that the diagram is of the γ-loop type.

(*d*) *The system iron–chromium*

The results of the thermal analyses are shown in table A3 and figure 10. The chromium used was high purity electrolytic flake metal supplied by Johnson, Matthey and Co. Ltd; the purity was greater than 99·98 %, and the oxygen content less than 0·002 %. The

metals were melted together *in vacuo* in the cooling-curve furnace, and were treated with dry hydrogen for 20 to 30 min, after which the cooling curve was taken *in vacuo*. For the alloys of higher chromium content, the temperature was raised to 1600 to 1630° C during melting, with a slight loss of both metals by volatilization, and a decrease in the chromium content of the alloy. Experiments with alloys melted *in vacuo* and in argon showed that this loss occurred almost entirely before the arrest point, and so did not affect the accuracy if the ingot were analyzed.

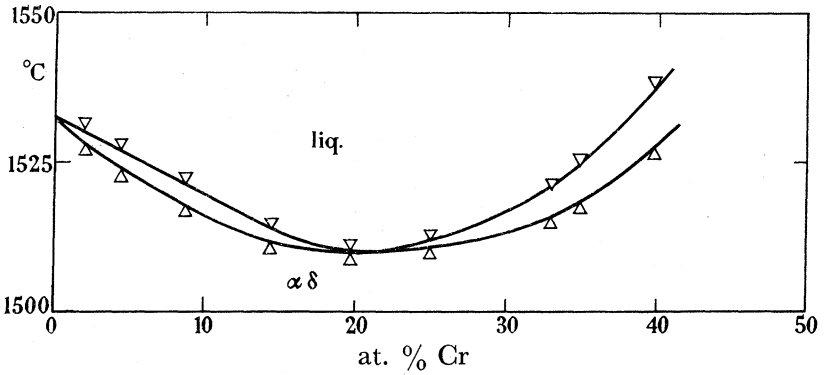

FIGURE 10. Liquidus and solidus curves for Fe–Cr, from 0 to 40 at. % Cr.

The equilibrium diagram of the system Fe–Cr is of the γ-loop type, with continuous solid solutions between the body-centred cubic chromium and the α-iron, whilst a σ-phase is formed at low temperatures in the equiatomic region. The present results indicate that the liquidus and solidus curves pass through a minimum in the region of 20 to 21 at. % Cr, in good agreement with the diagram of Adcock (1931), but the present data give a much narrower freezing range than those of Adcock, whose thermal analyses were carried out in an induction furnace.

(*e*) *The system iron–manganese* (*iron-rich alloys*)

The results of the thermal analyses are shown in table A4 and figure 11. The manganese used was electrolytic flake metal of 99·9 % purity supplied by Johnson, Matthey and Co. Ltd, and for work on iron-rich alloys the manganese was treated in a current of hydrogen at 1100 to 1200° C. After thorough degassing, the alloys were melted in the cooling-curve furnace under argon containing a trace of hydrogen, and the same atmosphere was used for thermal analysis in the apparatus of figure 1. Under these conditions the loss of manganese was negligible, and little difficulty was encountered.

On the iron-rich side, the equilibrium diagram of the system Fe–Mn is of the open γ-field type, and a continuous series of solid solutions extends between γ-Fe and γ-Mn. The thermal arrests for the iron-rich alloys were generally good, although thermal hysteresis occurred on the γ/δ boundary. On cooling curves, the arrests for the peritectic horizontal also showed considerable supercooling, and these points have been omitted from figure 11, although they are included in table A4. From the melting-point of iron, the liquidus and solidus of the δ-phase fall fairly steeply to 1472° C, the temperature of the peritectic reaction: $\delta\ (9{\cdot}6) + \text{liquid}\ (13{\cdot}0) \rightleftharpoons \gamma\ (10{\cdot}2)$.

From this temperature the liquidus and solidus curves of the γ-phase continue to fall until a minimum value is reached at about 13 at. % Fe; these alloys are dealt with in § 5.

The previous equilibrium diagram for iron-rich alloys (Smithells 1955) is due essentially to Gayler (1933), who placed the γ/δ peritectic horizontal at 1504° C, mainly as the result of microscopical work. Arrests at a somewhat lower temperature were noted, but could not be interpreted, although from the present results there seems little doubt that these

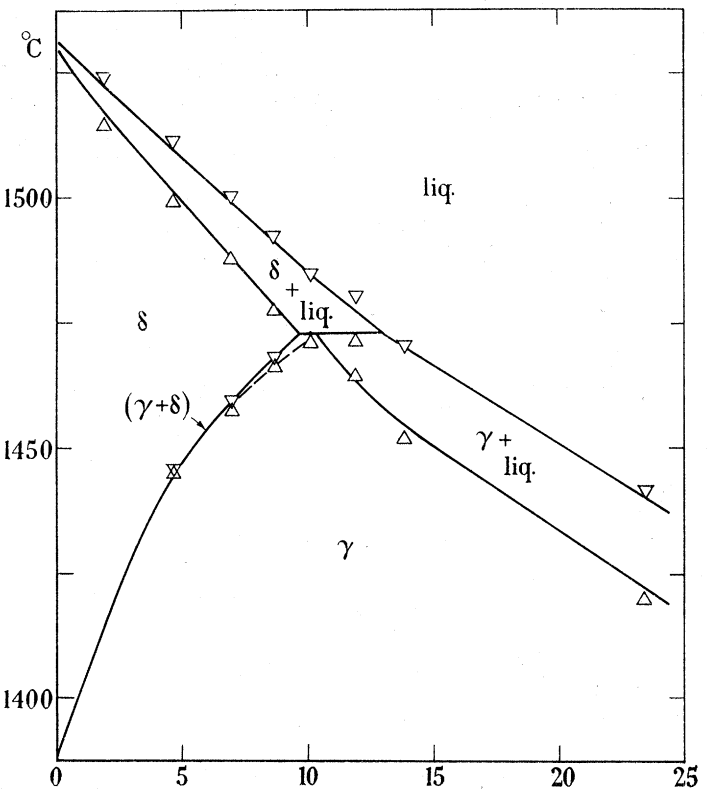

FIGURE 11

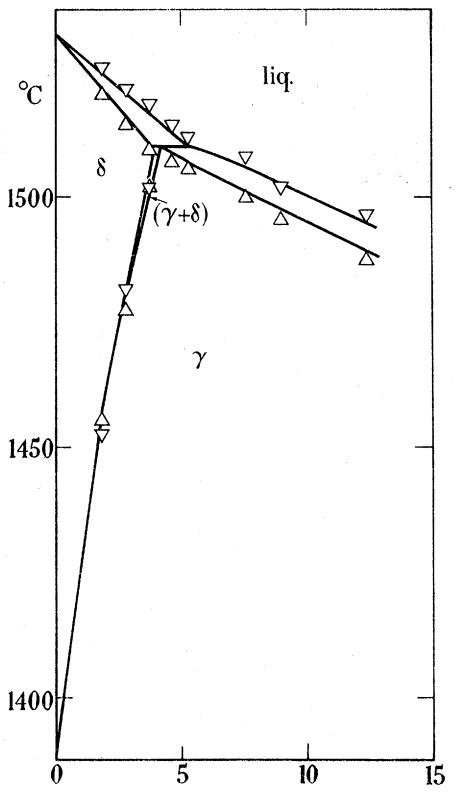

FIGURE 12

FIGURES 11 AND 12. Phase diagrams for Fe–Mn and Fe–Ni in the region of the δ-field and the δ/γ peritectic.

were really due to the peritectic horizontal. When compared with the results of Gayler, the present work indicates a much narrower freezing range for the δ-solid solution, and a greater solubility of manganese in δ-iron.

(*f*) *The system iron–nickel*

The results of the thermal analyses are shown in table A 5 and figure 12. The nickel used was specially pure nickel shot kindly presented by the Mond Nickel Co. Ltd. The alloys were melted in hydrogen, after which the furnace was evacuated, and the cooling curve taken *in vacuo*, using standard methods, except that inoculation with filings was employed in order to reduce supercooling.

The equilibrium diagram of the system Fe–Ni is of the open γ-field type, and the δ-liquidus and solidus curves fall smoothly to a peritectic horizontal at 1511° C corresponding to the reaction

$$\text{liquid } (5{\cdot}2) + \text{solid } \delta\ (3{\cdot}8) \rightleftharpoons \text{solid } \gamma\ (4{\cdot}1).$$

The peritectic temperature was confirmed by a double bend in the cooling curve for alloy 4·62, and by the intersection of the line for the δ/γ transformation with the solidus curve.

Of the earlier diagrams of iron-rich Fe–Ni alloys, the most accurate is that of Bristowe (1939), whose iron was probably slightly less pure (the oxygen and nitrogen content not being stated) than that in the present research. When Bristowe's data are adjusted to refer to a melting-point of 1532° C for pure iron, the present peritectic temperature (1511° C) is in good agreement with that of Bristowe (1510° C), but the present freezing ranges for the δ- and γ-solid solutions are only about one-third and one-half of those given in Bristowe's diagram.

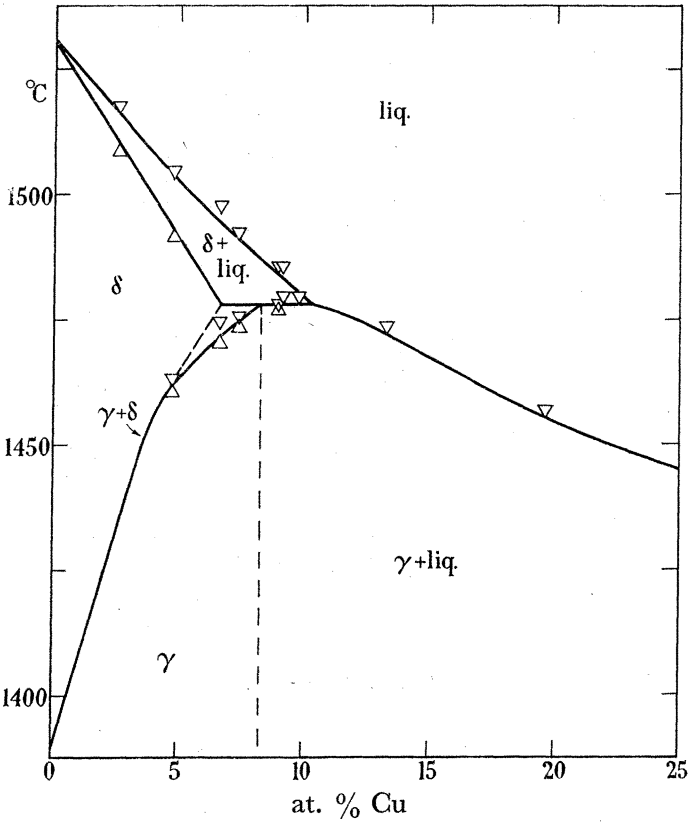

FIGURE 13. Phase diagram for Fe–Cu in the region of the δ-field and δ/γ peritectic.

(*g*) *The system iron–cobalt*

For convenience the results of the thermal analyses of Harris & Hume-Rothery (1953) are shown in table A 6.

(*h*) *The system iron–copper*

The results of the thermal analyses are shown in table A 7 and figure 13. The copper used was specially pure (>99·98 %) metal kindly presented by the British Non-Ferrous Metals Research Association. Appreciable amounts of copper were lost by volatilization if experiments were carried out *in vacuo* at 1500° C, and the methods adopted were therefore similar to those used for iron–manganese alloys.

The equilibrium diagram of the system Fe–Cu is of the expanded γ-field type with a restricted solubility of copper in γ-iron. The present work confirms the general form of

the equilibrium diagram determined by Maddocks & Claussen (1936), but indicates a narrower freezing range for the δ-phase. The temperature of the γ/δ peritectic was determined as 1478° C, in good agreement with the value 1477° C given by Ruer (1927), but slightly lower than the value 1481° C given by Maddocks & Claussen (1936). The peritectic horizontal corresponds to the reaction

$$\delta\ (6{\cdot}7) + \text{liquid}\ (10{\cdot}3) \rightleftharpoons \gamma\ (8{\cdot}3).$$

Annealing experiments at 1260 to 1270° C showed alloy 7·15 to be homogeneous, whilst alloy 8·5 contained traces of chilled liquid. This agrees with the diagram of Maddocks & Claussen, according to which the solidus of the γ-phase falls almost vertically from the peritectic temperature. Annealing experiments on alloy 19·68 at 1515 to 1530° C also confirmed the conclusion of Maddocks & Claussen that no region of liquid immiscibility exists.

5. Experimental results for manganese alloys

(*a*) *General*

For the work on manganese alloys, use was made of pure electrolytic flake metal supplied by Johnson, Matthey and Co. Ltd. This metal was of 99·9 % purity, and in the early work on iron–manganese alloys, the manganese was given a treatment in hydrogen at about 1100° C. It was found that this treatment did not affect the transition points but, in view of the results described below, the practice was discontinued for the later work. Johnson, Matthey and Co. Ltd also supplied some specially selected and purified manganese of 99·99 % purity which was used for work on the pure metal. For abbreviation this will be referred to as 'P' manganese, to distinguish it from the ordinary or 'C' metal of 99·9 % purity. Manganese dissolves hydrogen in the solid state (Potter & Lukens 1947), and on heating *in vacuo* most of this is driven off between 800 and 900° C, but some persists until melting when a further evolution takes place. The thermal arrests for the liquidus and solidus points of manganese alloys were in general well marked, and were easily interpreted except for the double arrests near the solidus referred to on p. 425.

The arrests for the δ/γ transformations at the higher temperatures were also satisfactory, but at the lower temperatures the γ/β transformations showed temperature hysteresis, and the results are approximate only.

Unless otherwise stated, the metals alloyed with manganese were from the same sources as those described for the work on iron alloys.

(*b*) *Pure manganese*

Experiments were made in which the whole process of melting and thermal analysis was carried out (*a*) under hydrogen, and (*b*) under argon, and (*c*) in other experiments the metal was melted under hydrogen which was then replaced by argon. The freezing-point of manganese in an atmosphere of argon was found to be reproducible at 1244 to 1245° C, whilst the value in hydrogen was about 3° C lower (1241° C). The same difference persisted in manganese-rich alloys, and as soon as this point had been established all thermal analyses were carried out in argon, and the previous treatment of the 'C' manganese with hydrogen was discontinued. The temperatures of the δ/γ (1135° C) and γ/β (1095° C) agreed with those of previous investigators (see Sully 1955) to within 3° C.

These transition temperatures were not affected by an atmosphere of hydrogen, although the use of this gas made the arrests less definite owing to the increased heat exchange between the assembly and the furnace. No difference was noted between the values obtained for the 'P' and 'C' grades of manganese. All tables of results for manganese alloys in Appendix A refer to experiments under argon.

(*c*) *The system manganese–titanium*

The results of the thermal analyses are shown in table A 8 and figures 14 and 15. Alumina refractories were satisfactory for alloys containing up to 25 at. % Ti, but beyond this point use was made of thoria crucibles, and of thoria-lined alumina thermocouple sheaths. The alloys were prepared in the cooling-curve furnace, which was slowly heated to about 1000° C with precautions to avoid allowing the pressure to rise above 10^{-3} mm Hg. The furnace was then filled with argon for the melting and thermal analysis.

Titanium is soluble in δ-Mn and the liquidus and solidus curves for the δ-solid solution fall to a eutectic horizontal at 1204° C, at which temperature the liquid (9·5) is in equilibrium with δ (7·5) and with the first intermediate phase which is probably Mn_3Ti. This phase is formed by a peritectic reaction between 1230 and 1250° C, and the liquidus then continues to rise to a maximum at 1325° C, at which temperature the compound Mn_2Ti is in equilibrium with the liquid. This part of the diagram was not examined in detail. Alloys in the range 33 to 50 at. % Ti showed a secondary arrest at 1181° C which may be identified with the ($Mn_2Ti+\beta$-Ti) eutectic placed at 1175° C by Hansen *et al.* (1953).

On the manganese-rich side of the diagram, the thermal analyses showed that titanium lowers the temperature of the γ/δ, and raises that of the γ/β transformation, with the formation of a closed γ-field (figure 15). Although not proved conclusively, it seems almost certain that the δ-phase of composition 0·6 to 0·8 at. % Ti undergoes a eutectoid decomposition at 1120° C to form a mixture of γ and β. The β/δ boundary rises with increasing titanium content, and a marked change in the form of the arrests suggested that the β-phase undergoes a peritectoid decomposition at about 1148° C. Microscopical investigation shows that the limit of solid solubility in the β-phase is about 3 at. % at 1100° C. The ($\gamma+\delta$), ($\gamma+\beta$) and ($\delta+\beta$) fields are too narrow to be shown on the scale of figure 14, and the homogeneous fields are shown separated by single lines.

The existence of a compound corresponding to Mn_3Ti is inferred only from thermal analyses, and remains to be substantiated by microscopical and X-ray evidence.

(*d*) *The system manganese–vanadium*

The results of the thermal analyses are shown in table A 9 and figures 16 and 17. This system was investigated by thermal analysis only, the metals being melted in alumina crucibles under argon after thorough degassing at about 1000° C. The arrests for the liquidus, solidus and γ/δ transformations were clear and satisfactory, but the β/δ transformations became increasingly sluggish in alloys with more than 5 at. % V.

The liquidus and solidus curves of the δ-phase are raised by the addition of vanadium (see figure 15), and a closed γ-field is produced which does not extend beyond 0·6 to 0·8 at. % V (figure 17). It is probable that the β-phase undergoes a peritectoid transformation ($\beta \rightleftharpoons \gamma+\delta$) at about 1107° C, but the two-phase fields were too narrow for this

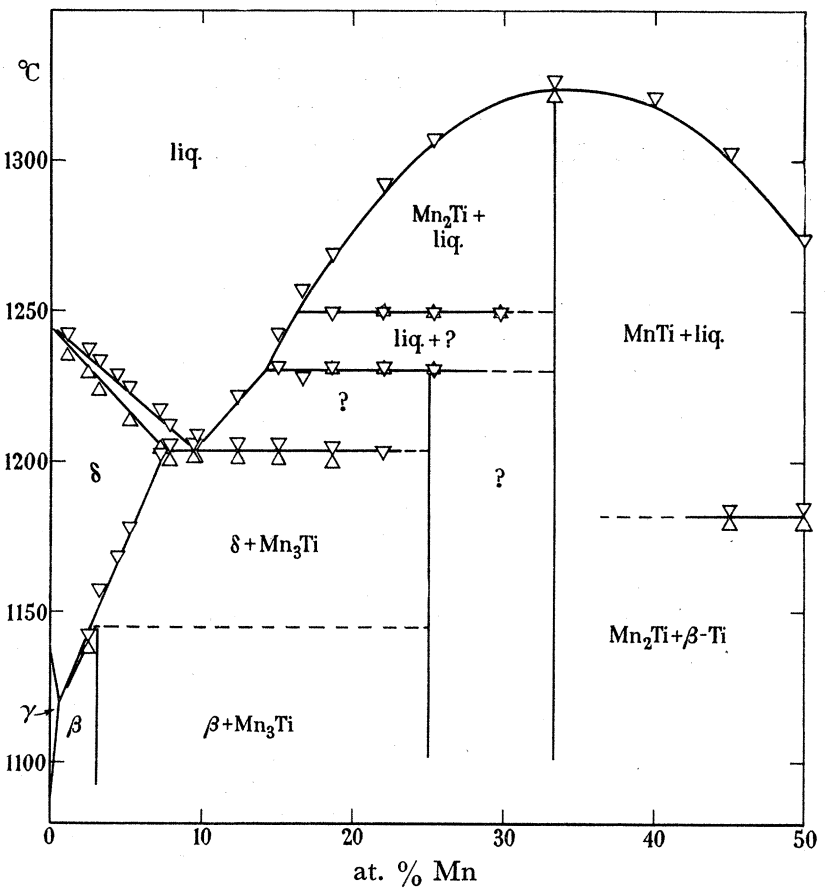

FIGURE 14. Phase diagram for Mn–Ti above 1100° C, and from 0 to 50 at. % Ti.

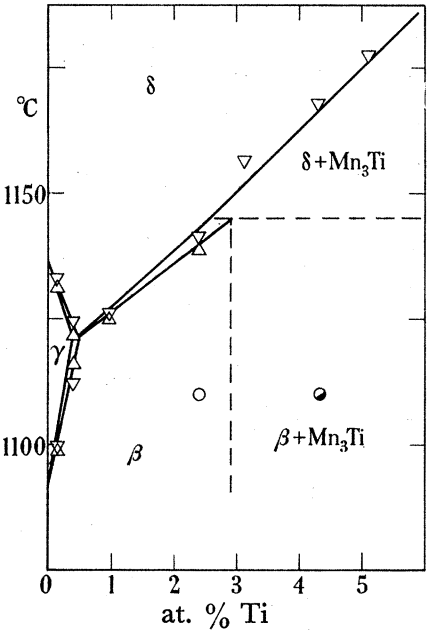

FIGURE 15. Phase diagram for Mn–Ti in the region of the γ-field and β/δ peritectoid.
○ one phase; ◕ two phase.

PHILOSOPHICAL TRANSACTIONS OF THE ROYAL SOCIETY A MATHEMATICAL, PHYSICAL & ENGINEERING SCIENCES

to be established in detail. Beyond the peritectoid point, the β/δ transformation is lowered by further addition of vanadium, and the δ-phase undergoes a eutectoid ($\delta \rightleftharpoons \beta + \sigma$) decomposition, the position of the eutectoid point being approximately 7·5 at. % V and 1020° C. There is no previous equilibrium diagram for the manganese-rich portion of this system, although the work of Pearson & Christian (1951) has established the existence of a phase with a typical σ-structure.

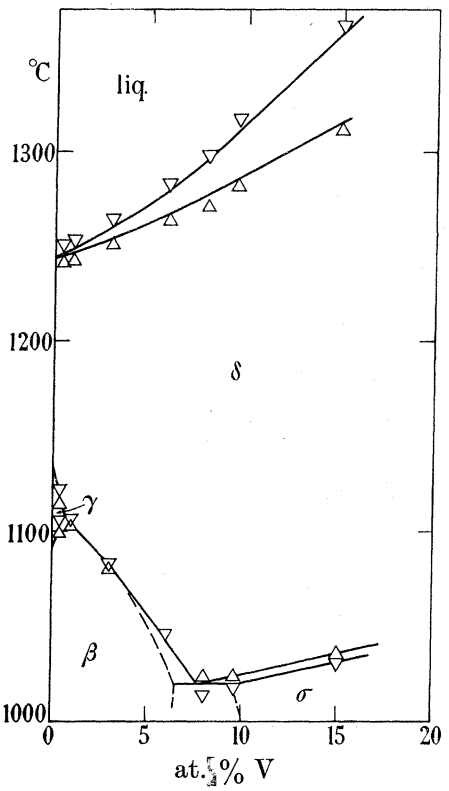

FIGURE 16. Phase diagram for Mn–V above 1000° C, from 0 to 15 at. % V.

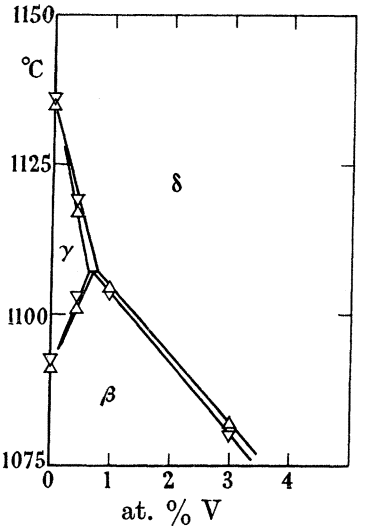

FIGURE 17. Closed γ-field in Mn–V.

(e) *The system manganese–chromium*

The results of the thermal analyses are shown in table A10 and figures 18 and 19. The system was examined by thermal analysis only, using the standard technique with alumina crucibles.

The liquidus and solidus curves of the δ-phase are raised by the addition of chromium, and there is a closed γ-field (see figure 18) extending to about 0·85 at. % Cr at 1110° C. As in the previous system, it is probable that the β-phase undergoes a peritectoid decomposition, but the two-phase fields were too narrow for this to be established in detail. Beyond the peritectoid point, the β/δ transformation falls with increasing chromium content until a eutectoid ($\delta \rightleftharpoons \beta + \sigma$) transformation occurs at 10·5 at. % Cr and approximately 1000° C (figures 18 and 19).

The present results disprove the diagram of Zwicker (1949), according to which the freezing-point of manganese is lowered by the addition of chromium, with the formation of a eutectic type of diagram. The present liquidus and solidus points agree well with those of Carlile, Christian & Hume-Rothery (1949), but show that these authors were

incorrect in drawing a steeply rising γ/δ transformation curve to meet a supposed γ/δ peritectic horizontal. The diagram of Carlile *et al.* is shown in figure 20, and it is now clear that what these authors regarded as the γ-eutectoid point was really the δ-eutectoid point, and the two-phase ($\sigma+\gamma$-Mn) field of these workers* is really the ($\sigma+\delta$-Mn) two-phase field. When these changes are made, and the closed γ-field is inserted, the present results can be reconciled with those of Carlile *et al.*, and the work was therefore not continued beyond the stage of figure 18.

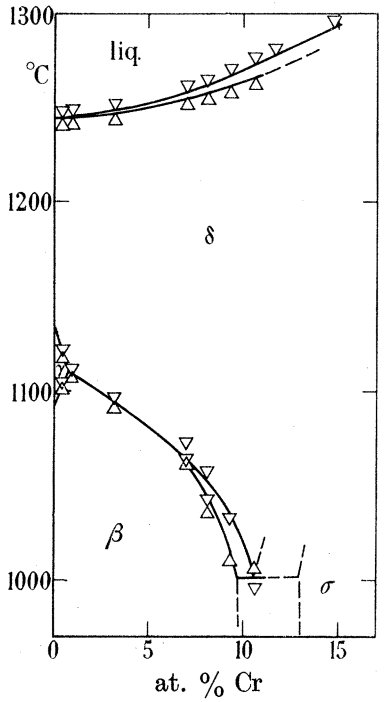

FIGURE 18. Phase diagram for Mn–Cr above 1000° C, from 0 to 12 at. % Cr.

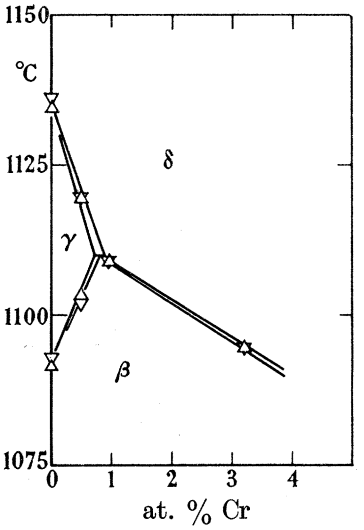

FIGURE 19. Closed γ-field in Mn–Cr.

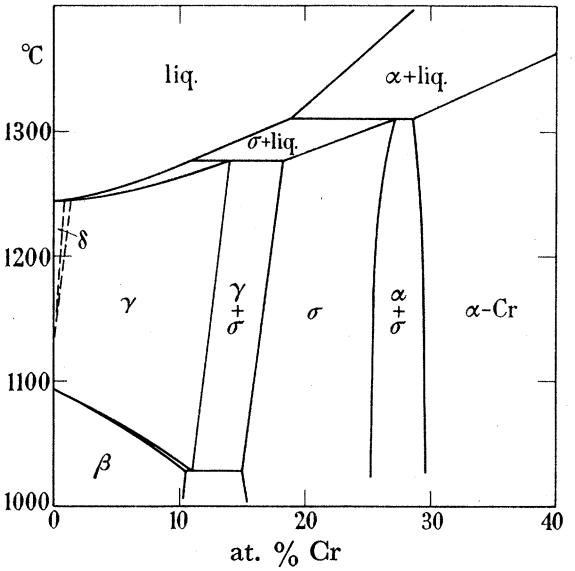

FIGURE 20. Phase diagram for Mn–Cr (after Carlile *et al.* 1949).

* In the diagram of Carlile, Christian & Hume-Rothery the σ-phase was denoted θ.

(*f*) *The system manganese–iron*

The results for the iron-rich alloys have been described previously (p. 430). With increasing manganese content the liquidus and solidus curves for the γ-phase continue to fall (figure 21) until a minimum is reached at 1232° C and 13 at. % Fe. At this point, to

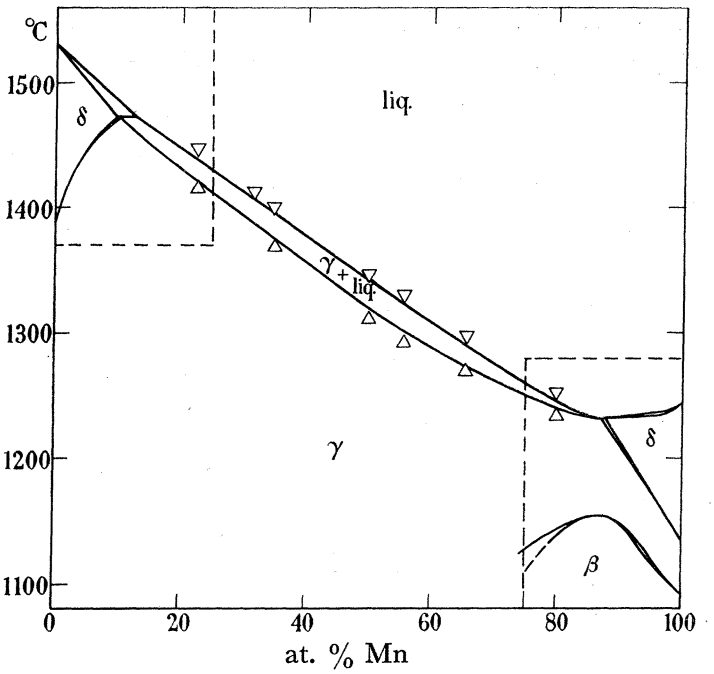

FIGURE 21. Phase diagram for Fe–Mn above 1100° C, showing arrests for centre of diagram. The dotted rectangles show the parts of the diagram given in Figures 11 and 22.

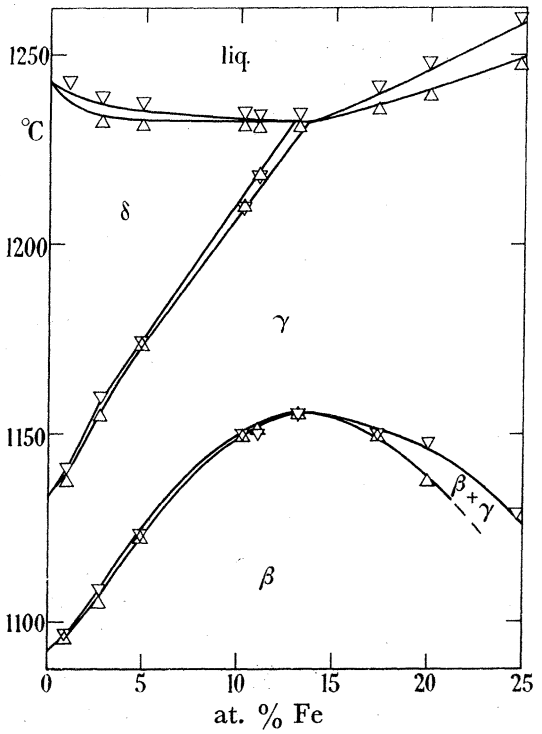

FIGURE 22. Phase diagram for Mn–Fe above 1100° C, from 0 to 25 at. % Fe.

within the limits of accuracy of the present methods, the γ-phase liquidus and solidus curves coincide, and the liquidus curve then rises to the melting-point of δ-Mn (figure 22), which dissolves up to 12 at. % Fe. The freezing range of the δ-Mn solid solutions is very narrow. It seems probable that the minimum at 1232° C is a eutectic point at which the solid phases are the δ-Mn solid solution, and the γ-phase whose composition is almost exactly the same as that of the liquid (figure 22), but the possibility of a peritectic horizontal with a minimum in the freezing-point curve on the iron-rich side cannot be entirely disproved. The data are given in table A 11.

The temperature of the δ-Mn/γ-Mn transformation is raised by the addition of iron, whilst that of the γ-Mn/β-Mn transformation is first raised, and then passes through a maximum at 1155° C and 13 at. % Fe, beyond which the transformation temperature falls. (The temperature of the β-Mn/α-Mn transformation is only slightly lowered by the addition of iron, and the β-Mn phase undergoes a eutectoid decomposition ($\beta \rightleftharpoons \alpha + \gamma$) at about 700° C.)

When compared with previous work (Smithells 1955) the present γ-liquidus curve falls smoothly, and does not show the bend in the region of 60 at. % Mn shown in the earlier diagrams. At the manganese-rich end of the diagram, the present work is the first which has firmly established the relation between the δ-Mn and γ-Mn fields.

(*g*) *The system manganese–cobalt*

The results of the thermal analyses are shown in table A12 and figure 23. The cobalt used was spectrographic standardized sponge provided by Johnson, Matthey and Co. Ltd.

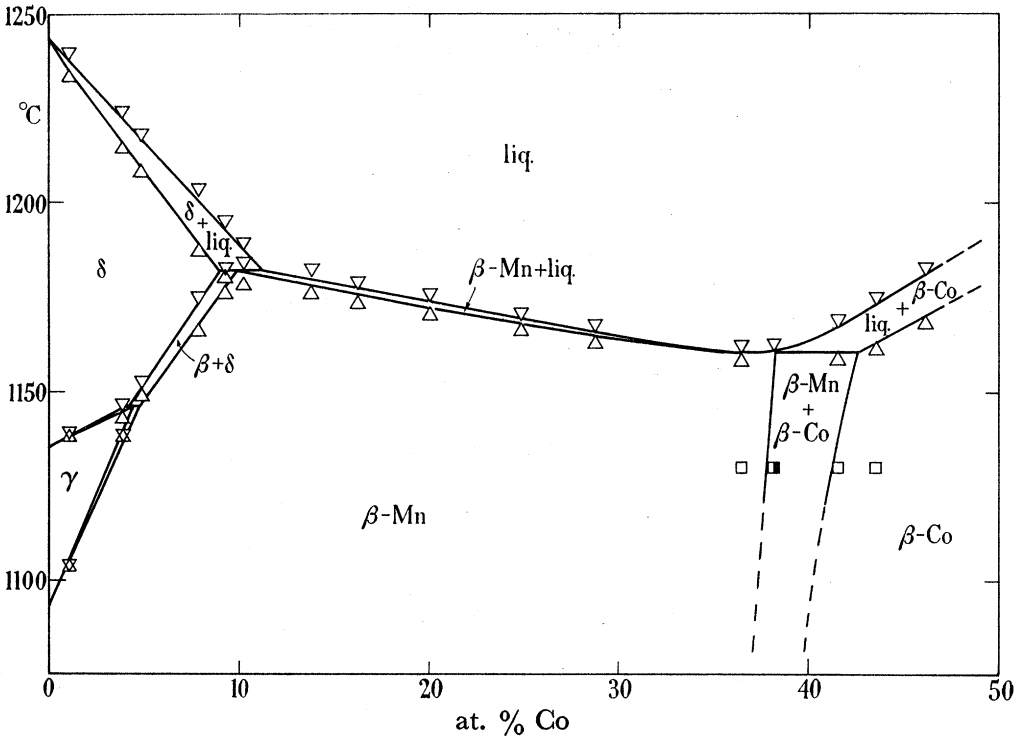

FIGURE 23. Phase diagram for Mn–Co above 1050° C, for 0 to 50 at. % Co.
□ one phase; ◨ two phase

The sponge was mixed with the manganese flake and degassed in the usual manner, but the process was slow, and special precautions were taken to prevent the pressure from rising above 10^{-3} mm Hg.

The addition of cobalt to manganese produces a fall in the δ-liquidus and solidus curves, and a rise in the temperature of the δ/γ transformation. At the same time the temperature of the γ/β transformation rises even more steeply, so that the γ-field is closed by a peritectoid reaction as shown in figure 23. From this point, the boundaries of the δ-Mn and β-Mn fields rise with increasing proportions of cobalt, until the β-Mn phase comes into equilibrium with the liquid phase, and at 1182° C the σ-Mn and β-Mn fields are connected by a peritectic horizontal, corresponding to the reaction

$$\text{liquid (11·2 at. \% Co)} + \delta\text{-Mn (9·0 at. \% Co)} \rightleftharpoons \beta\text{-Mn (10 at. \% Co)}.$$

The freezing range of the β-Mn phase is very narrow, and the liquidus and solidus continue to fall to a minimum at 36 to 37 at. % Co and 1160° C. This minimum is barely separable from a peritectic horizontal at 1161° C where the β-Mn phase decomposes into a mixture of liquid and of the solid solution in the f.c.c. β-Co (figure 23). The boundaries between the solid phases below the peritectic temperature were determined by microscopical methods, and confirmed by X-ray powder photographs. The previously accepted equilibrium diagram (Smithells 1955) shows a continuous range of solid solutions between γ-Mn and β-Co, and is quite incorrect in this, and in other respects. The present diagram is, however, partly in agreement with some unpublished work by J. W. Christian (1956). It is to be noted that the anomalous arrests on heating curves below the solidus referred to on p. 425 were not found for the solidus curve of the β-Mn phase.

(*h*) *The system manganese–nickel*

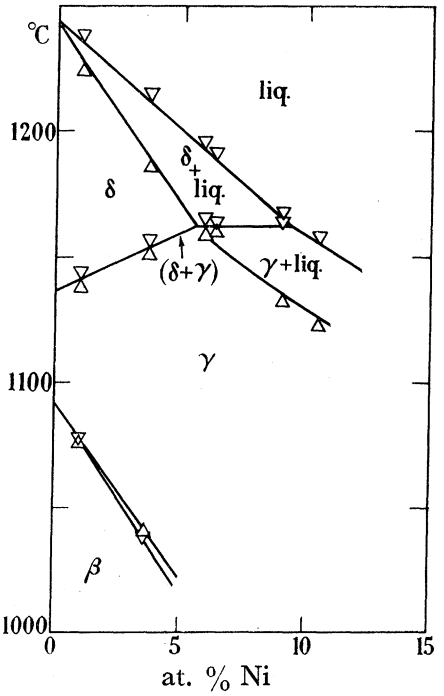

FIGURE 24. Phase diagram for Mn–Ni for 0 to 12 at. % Ni [$(\gamma+\delta)$ region drawn as a single line].

The results of the thermal analyses are shown in table A13 and figure 24. The metals were degassed and melted under argon, using the standard technique. The effect of adding nickel to manganese is to lower the temperatures of the α/β and β/γ transformations, and to raise that of the γ/δ transformation. The liquidus and solidus of the δ-Mn phase fall steeply to a peritectic horizontal at 1162° C, corresponding to the reaction

$$\text{liquid (9·2 at. \% Ni)} + \delta\text{-Mn (5·5 at. \% Ni)} \rightleftharpoons \gamma\text{-Mn (5·6 at. \% Ni)}.$$

The present results are in agreement with those of Coles & Hume-Rothery (1951), who, however, failed to observe the arrests for the peritectic horizontal, the existence of which was inferred only from a change in the slope of the liquidus.

(*i*) *The system manganese–copper*

The results of the thermal analyses are shown in table A14 and figure 25, and were obtained by the standard technique in an atmosphere of argon. The liquidus and solidus curves for the δ-Mn phase fall steeply to 1098° C, at which temperature there is a horizontal corresponding to the reaction (see figure 25)

$$\delta\text{-Mn (12·5 at. \% Cu)} \rightleftharpoons \text{liquid (24 at. \% Cu)} + \gamma\text{-Mn (11·8 at. \% Cu)}.$$

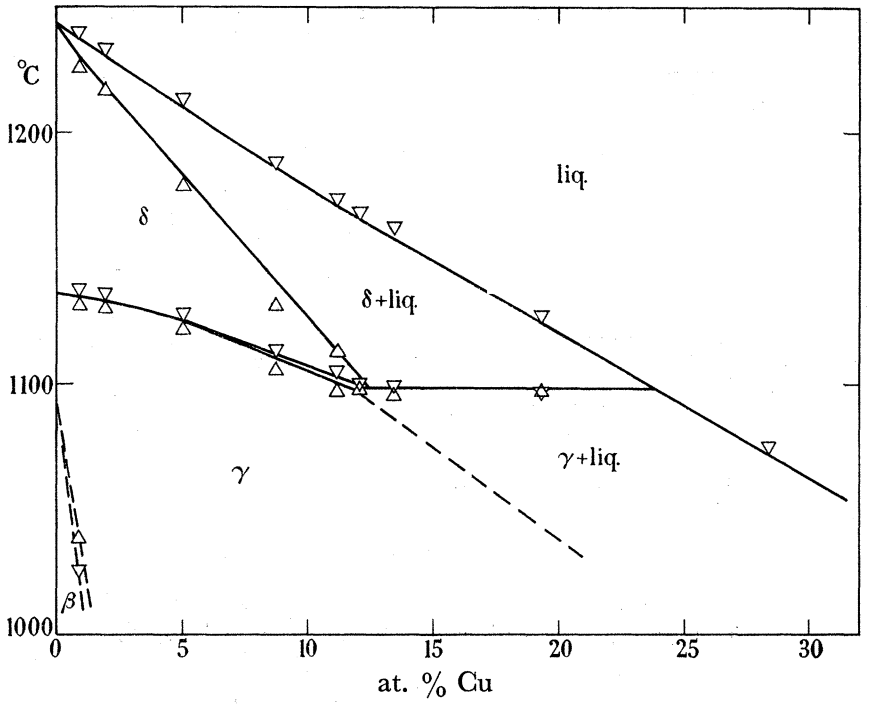

FIGURE 25. Phase diagram for Mn–Cu above 1000° C, from 0 to 30 at. % Cu.

Beyond this point the liquidus continues to fall, and the diagram has been well established by previous workers (Smithells 1955). There is no appreciable solid solubility of copper in either α-Mn or β-Mn.

5. Discussion

(i) *The equilibrium diagrams of iron and manganese alloys*

(*a*) *General*

The equilibrium diagrams of the iron and manganese alloys are summarized in figures 26 to 28, in which, owing to the small scale, some of the two-phase regions are represented by single lines.

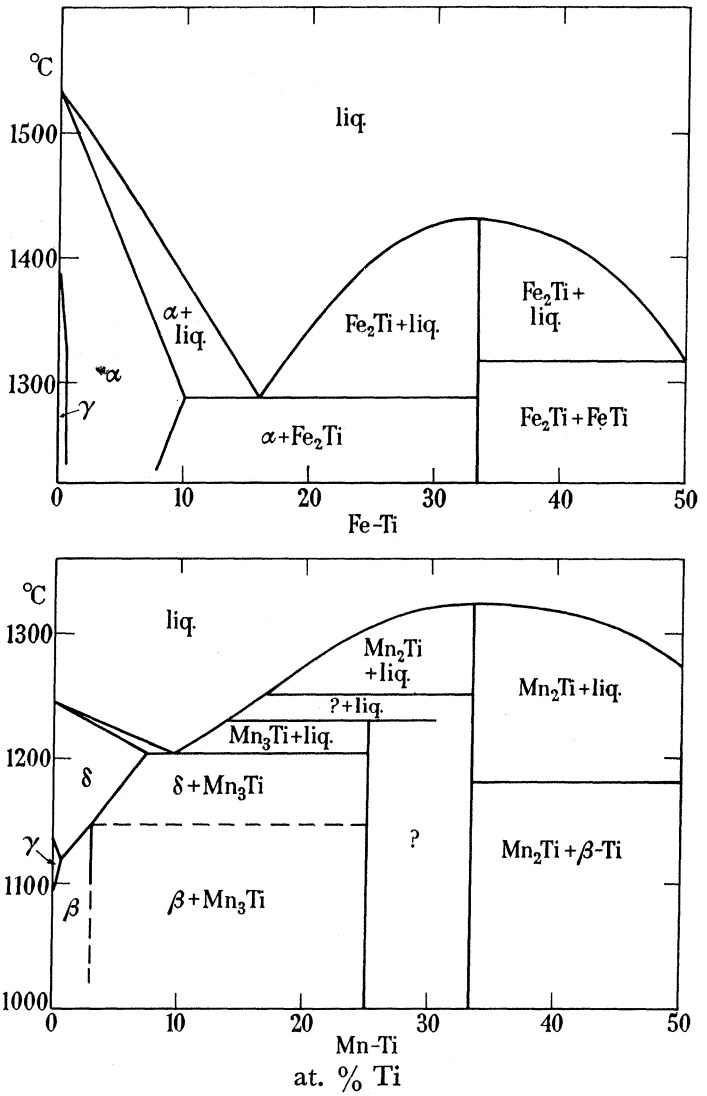

Figure 26. Phase diagrams for Fe–Ti and Mn–Ti.

For the iron alloys with the elements concerned, the size factors are very favourable for Mn, Co, Ni and Cu, and are well within the favourable zone for V (size factor+6 %), but Ti (size factor+15 %) lies on the border of the unfavourable zone as defined by the work of Hume-Rothery and his collaborators (Hume-Rothery & Raynor 1954). The atomic diameter of Mn and its δ- and γ-modifications is slightly larger than that of Fe, and results in the size factor being very favourable in the whole series of elements V, Cr, Fe, Co, Ni and Cu, whilst with Ti the size factor is considerable (+10 %), but still within the favourable zone. The crystal structures of β-Mn and α-Mn involve closest distances of

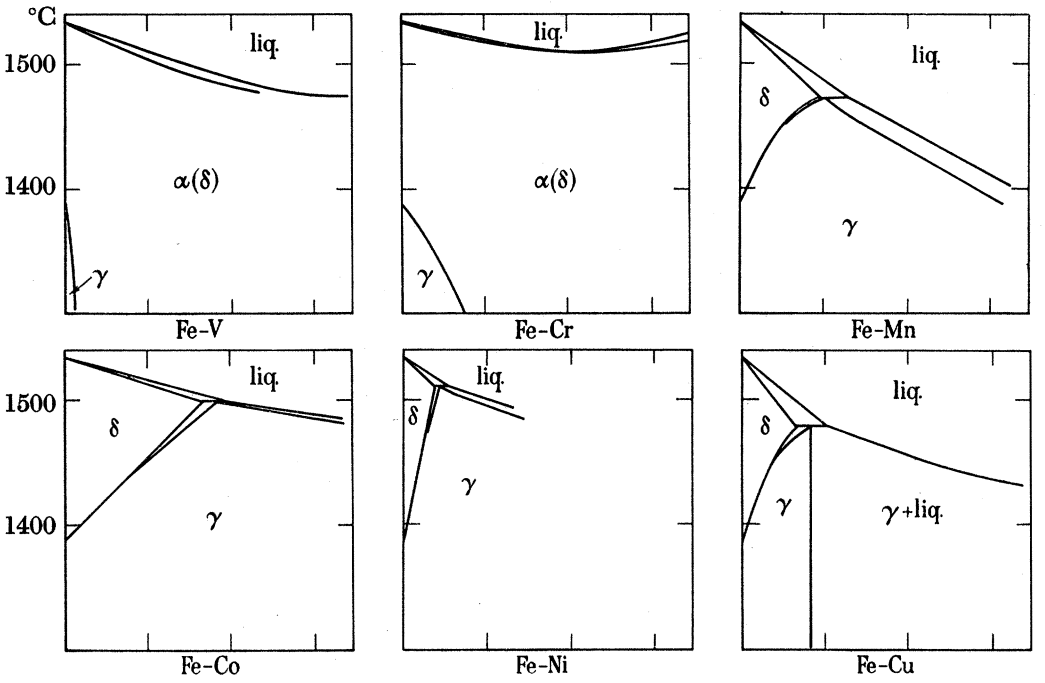

FIGURE 27. Comparison of iron-rich diagrams with elements from V to Cu. Temperature scale in 100° C intervals and composition scale in 10 at. % intervals.

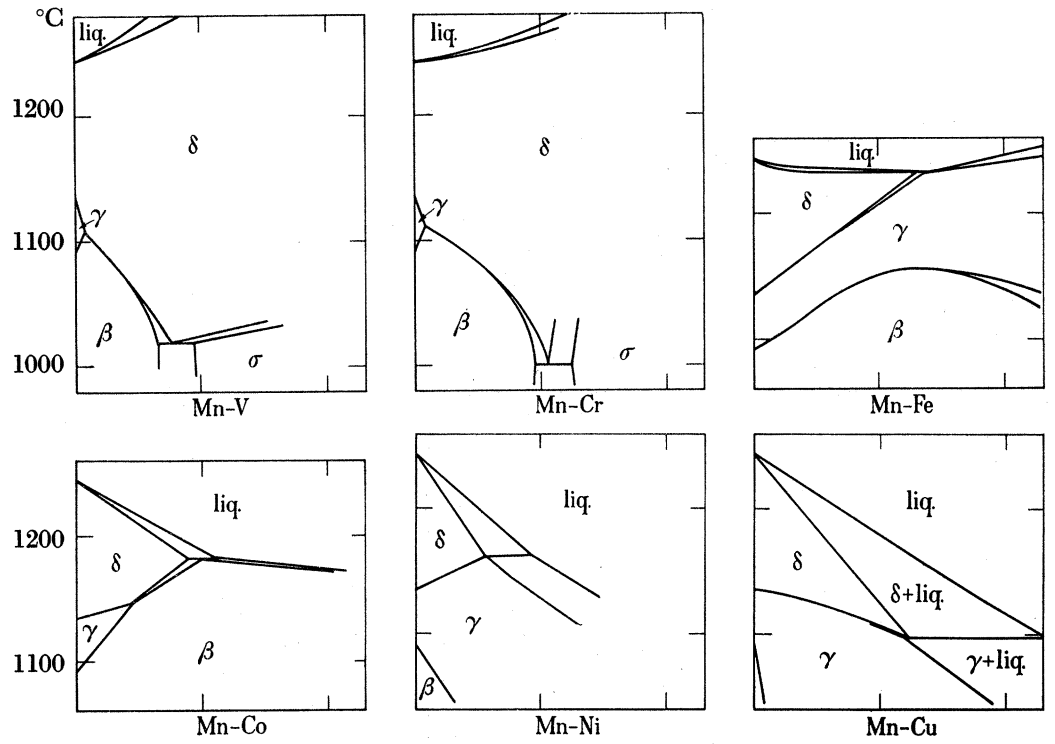

FIGURE 28. Comparison of manganese-rich diagrams with elements from V to Cu. Narrow two-phase regions represented by single lines; temperature scale in 100° C intervals and composition scale in 10 at. % intervals.

PHILOSOPHICAL TRANSACTIONS OF THE ROYAL SOCIETY A MATHEMATICAL, PHYSICAL & ENGINEERING SCIENCES

approach of 2·38 and 2·24 Å respectively, and for these the atomic diameter of V (2·62 Å) is near the limit of the favourable zone, unless vanadium itself can undergo a change in electron configuration similar to that which gives rise to the abnormally close interatomic distances in α-Mn and β-Mn.

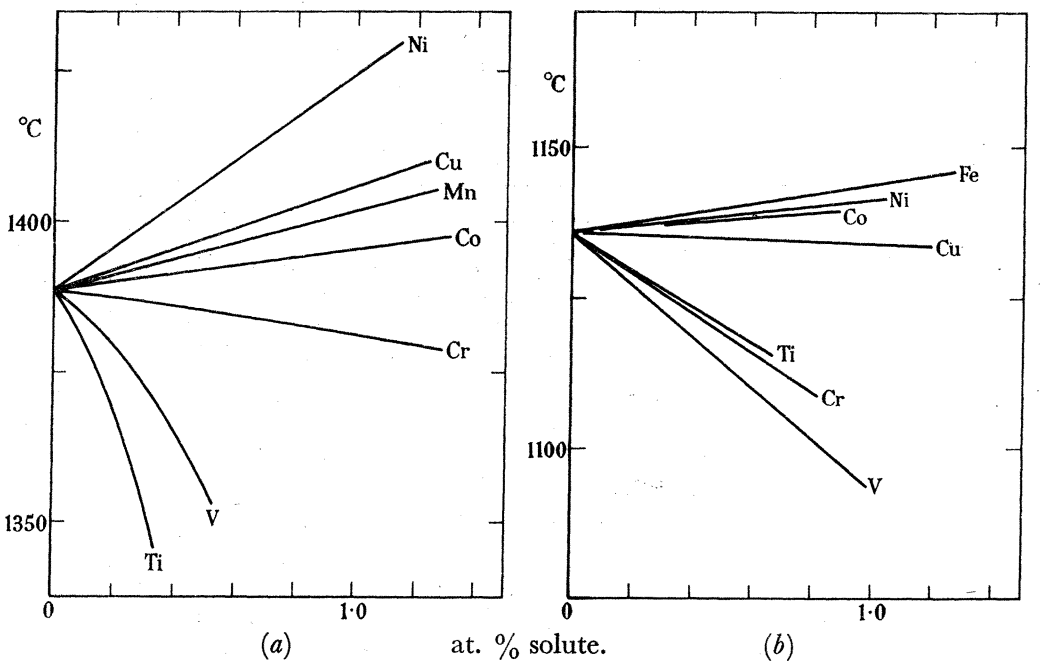

FIGURE 29. Mean initial slopes of γ/δ boundaries in (*a*) iron-rich alloys, and (*b*) manganese-rich alloys.

(*b*) *The $\delta \rightleftharpoons \gamma$ equilibrium and the extent of the γ-fields*

As explained on p. 418, the transformations $\delta \rightleftharpoons \gamma$ refer to the same crystalline structures in both Fe and Mn alloys, and the δ/γ boundaries are directly comparable. In the case of Fe alloys it is well known that metallic alloying elements can be divided into those which favour the γ-phase and give rise to equilibrium diagrams with open or expanded γ-fields, and those which favour the $\alpha(\delta)$ phase and give rise to 'γ-loops' or contracted γ-fields. This classification was due originally to Wever (1929), and was extended by Andrews (1952), but in spite of much discussion the relations are empirical and there is no satisfactory theory.*

Owing to the difference between the crystal structures of δ-Mn and β-Mn, the $\gamma \rightleftharpoons \beta$ transformation in Mn alloys is not structurally similar to the $\gamma \rightleftharpoons \alpha$ transformation in Fe alloys, and there is no possibility of the δ-Mn and β-Mn phase fields uniting to form a single field. There is, however, a remarkable correspondence between the effects of the different elements in stabilizing the γ-fields. In each series closed γ-fields are produced by Ti, V and Cr, whilst open or expanded γ-fields are produced by Mn (in Fe), Fe (in Mn) and Ni. In Fe alloys, an open γ-field results from the addition of Co, and in Mn alloys

* The recent attempt of Schubert (1955) to explain the effects in terms of an 'OrtsKorrelation' of electrons is unconvincing, because it depends ultimately on the assumption that with Cu and Zn as many as 11 and 12 of the outer electrons per atom are directly concerned with the cohesion, and that on passing to Ga the number sinks suddenly to 3.

the addition of cobalt raises the δ/γ boundary and stabilizes the γ-field at higher temperatures. At the same time, as explained below, the β-Mn field is greatly stabilized by Co, and a closed γ-field results from a raising of the γ-Mn/β-Mn boundary at lower temperatures.

Figure 29 shows that the δ/γ boundary in both manganese and iron alloys is depressed by Ti, V and Cr, and is raised by Mn (in Fe), Fe (in Mn), Co and Ni, whilst in each series the γ-stabilizing power of Ni is greater than would be expected from the behaviour of its immediate neighbours in the periodic table.

Copper behaves anomalously in both series of alloys. In the Fe alloys, it expands the γ-field, but the solubility in γ-Fe is restricted in spite of the favourable size factor. In the Mn alloys there is a continuous series of solid solutions between γ-Mn and Cu, but both δ/γ and γ/β boundaries are lowered, although as the relative lowering of the γ/β boundary is the greater, the γ-phase field is increased in extent.

The above facts suggest strongly that the tendencies for Ti, V and Cr to favour the body-centred cubic structure, and for Co, Ni and Cu to favour the face-centred cubic structure are real characteristics of the elements concerned, and do not depend on a balance of factors peculiar to iron.

(c) *The* γ-Mn $\rightleftharpoons$ β-Mn *equilibrium*

Figure 28 shows that, on passing from V $\rightarrow$ Cr $\rightarrow$ Mn $\rightarrow$ Fe $\rightarrow$ Co $\rightarrow$ Ni $\rightarrow$ Cu, the stability and range of the solid solutions in β-Mn increase to a maximum in the system Mn–Co, where the β-Mn phase persists to such a high temperature that it is in equilibrium with the liquid. This remarkable stability of the β-Mn phase is reflected in a γ/β boundary which rises so steeply that it intersects the δ/γ boundary, and so prevents the formation of a continuous series of solid solutions between γ-Mn and f.c.c. β-Co.

(ii) *Relative depressions of liquidus and solidus curves for solid solutions in* δ- *and* γ-Fe

Figure 30 shows the relative depressions of the liquidus and solidus curves, and also the freezing ranges for the solid solutions in δ-Fe. The effect of the large-size factor in the system Fe–Ti is apparent. The effect of Mn is anomalous, but for the remaining elements the relative depressions of liquidus and solidus curves follow well-defined sequences Ti$>$V$>$Cr and Co$<$Ni$<$Cu. This is the same general effect as that found by Sutton & Hume-Rothery (1955) for the relative lattice distortions produced by equi-atomic percentages of the same elements in α-Fe; and these effects appear to be simply related to the difference between the positions of solvent and solute in the periodic table. For the lattice distortions the behaviour of Mn was again anomalous.

Figure 31 shows the liquidus and solidus curves for the γ-solid solutions, and for the elements following Fe the depressions are again in the order Co$<$Ni$<$Cu, although the equilibrium in the system Fe–Cu is clearly different from that in the other systems. Comparison of the slopes for γ in figure 31 shows that the depressions of the Fe–Ni liquidus and solidus curves are relatively less than would be expected from the δ-liquidus and solidus data of figure 30. The tendency for Ni to stabilize the γ-phase to an extent greater than would be expected from the behaviour of adjacent elements in the periodic table is thus found for the $\gamma \rightleftharpoons$ liquid, as well as for the $\gamma \rightleftharpoons \delta$ equilibrium.

The diagrams below give the simple depressions of the liquidus and solidus curves relatively to the freezing-point of the pure metal. It is well known (Hildebrand & Scott 1950) that for an ideal solid solution between two metals of the same crystal structure, the liquidus and solidus curves give rise to a lens-shaped two-phase region, the exact form of which depends on the latent heats of fusion of the two metals. For a first simplified

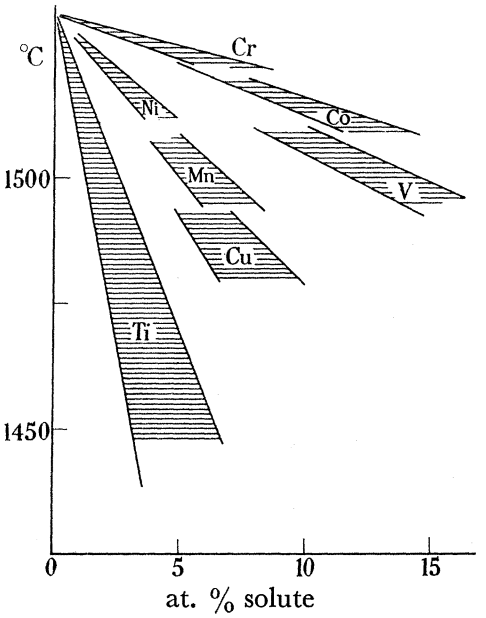

FIGURE 30. Slopes of δ-liquidus and solidus in iron-rich alloys.

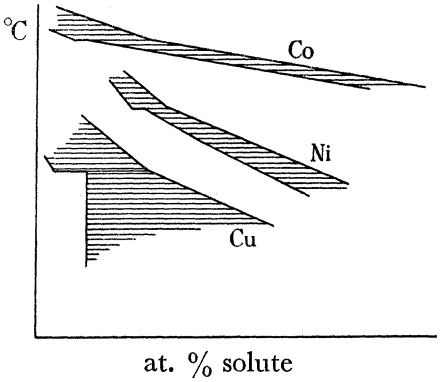

FIGURE 31. Change of slope at the γ/δ peritectic and freezing ranges for γ-solid solutions in iron-rich alloys. The curves for all three systems are plotted on the same scale, but have been shifted horizontally to allow easy comparison of the gradients in the region of the peritectics.

approximation we may join the freezing-points of the two metals by a straight line, to give what may be called the *linear s.l. curve*, and compare this with the line half-way between the liquidus and solidus curves for our alloys. In figure 32 we denote by ΔT the amount by which the 'half-way line' lies below the linear s.l. curve, and the relative values of ΔT for a given atomic percentage of solute are in the order Ti > V > Cr > Mn. The size-factor effect for Ti is again apparent, but the effect of Mn is now in accordance with its position in the periodic table. This suggests strongly that whatever electronic characteristic is responsible for the low melting-point of δ-Mn is also a characteristic of

Mn when alloyed with Fe. Similar curves cannot be drawn for Co, Ni or Cu because these do not crystallize in the body-centred cubic structure. However, if the γ-liquidus and solidus for the systems Fe–Co and Fe–Ni are considered, and the melting-point of γ–Fe is taken as 1520° C, (see p. 451) the deviation curves are as shown in figure 32.

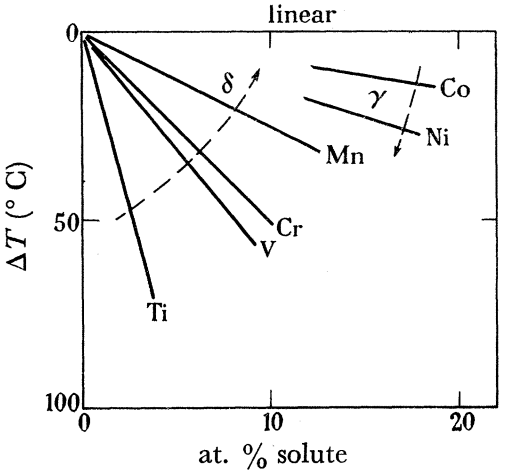

FIGURE 32. Initial deviations of mean δ-liquidus/solidus slopes from linear relation. γ-deviation also included for Fe–Co and Fe–Ni.

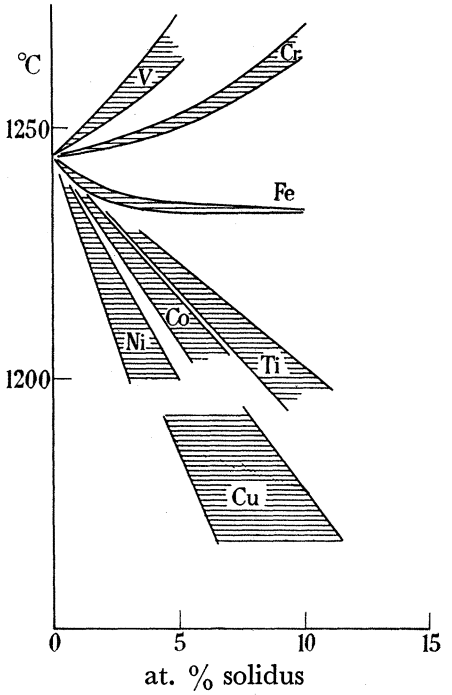

FIGURE 33. Slopes of δ-liquidus and solidus in Mn alloys.

(iii) *Relative depressions of liquidus and solidus curves for solid solutions in δ- and γ-Mn*

The more complicated form of the equilibrium diagrams (figure 28) for the Mn alloys means that only the δ-solidus and liquidus curves can be compared for the whole series of solute elements, and figure 33 shows the relative slopes of these curves. Ti (1660° C),

V (?1860° C) and Cr (1845° C) have very much higher melting-points than Mn, and this is reflected in the raising of the liquidus and solidus produced by V and Cr, the effect being in the order V > Cr. For these elements the size factor is very favourable, and it is presumably the much larger size factor in the system Mn–Ti which is responsible for the marked depression of the liquidus and solidus in this system. For the elements following Mn in the periodic table, the depression of the liquidus and solidus curves follow a well-defined sequence Fe < Co < Ni, but this is not continued by Cu.

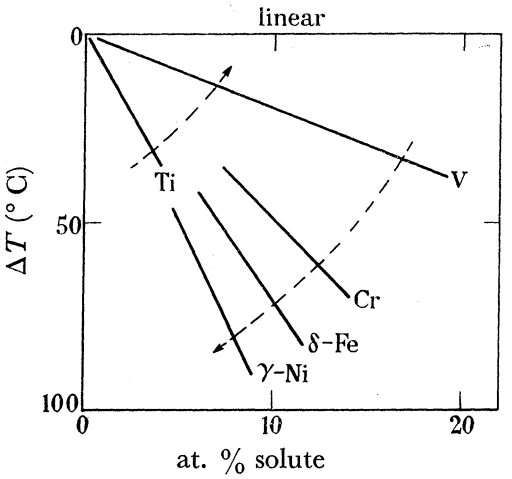

FIGURE 34. Initial deviations of mean δ-liquidus/solidus slopes from linear relation. γ-deviation also included for Mn–Ni.

It is again of interest to compare the slopes of the 'half-way' lines with those of the linear s.l. curves for the different system. Just as it is possible to regard the Fe alloys as based on the diagram of figure 36 with a hypothetical melting-point for pure γ-Fe, so the Mn-rich alloys may be regarded as based on an analogous diagram, with a hypothetical melting-point of ~1220° C for pure γ-Mn (this figure is obtained by extrapolation of the γ-curves for the system Mn–Ni). For both γ- and δ-phases the 'half-way' curves lie below the linear s.l. curves, and figure 34 shows the values of ΔT and is analogous to figure 32 for the Fe alloys. When plotted in this way, the effect of the large size factor in the system Mn–Ti is still apparent, but for the remaining elements there is a well-defined sequence in which at equiatomic percentages the depressions are in the order V < Cr < Fe < γ-Ni.* In contrast to the results for Fe alloys there is no suggestion of an effect increasing regularly with the distance between the solvent and solute in the periodic table. The results suggest strongly that, although Mn may be abnormal as a solvent, the remaining elements form a regular sequence from V to Ni. In general, a large size factor increases the depression of liquidus and solidus, and since for the δ-Fe alloys the equiatomic depression sequence is V > Cr, the size-factor effect in the system Fe–Ti tends to reinforce the presumably normal or electronic effect, with a resulting sequence Ti > V > Cr, in which the difference between the effects of Ti and V is abnormally great. For the δ-Mn alloys, on the other hand, where the sequence is V < Cr < Fe, the size-factor effect in the system Mn–Ti opposes the normal or electronic effect, and so the Ti curve in figure 34 is out of sequence.

* No value can be given for Co, because as shown in figure 28 the γ-Mn phase does not come into equilibrium with the liquid in the system Mn–Co.

(iv) *Van't Hoff's equation and the latent heats of fusion of* δ-Fe *and* δ-Mn

The thermodynamic data for Fe have been reviewed by Darken & Smith (1951), who give tables for free energies, entropies and enthalpies up to 1700° C. The ultimate sources of these data appear to be direct measurements of thermal capacities, and do not involve calculations from freezing-point or other transformation curves.* The latent heat of fusion is given as $3{\cdot}67 \times 10^3$ cal/mole.

If the liquid and solid solutions are monatomic, the latent heat of fusion of δ-Fe may be calculated from the gradients of the liquidus and solidus curves at infinite dilutions by means of Van't Hoff's equation, in the form

$$\frac{\mathrm{d}x_l}{\mathrm{d}T} - \frac{\mathrm{d}x_s}{\mathrm{d}T} = \frac{L}{RT_0^2},$$

where x_l and x_s are the atomic fractions of solute on the liquidus and solidus, and L and T_0 are the latent heat of fusion and melting-point (in ° K) of pure Fe. As explained on p. 423 the heating curve arrests for the 'H' iron were always about 1° C lower than the arrests on cooling curves. The tables of results give the observed values, but, in view of the above discrepancy, we think that for thermodynamic examination the most reasonable procedure is to raise the solidus point by 1° C so that both solidus and liquidus curves meet at 1533° C for zero concentration of solute. For $x_l = 0{\cdot}05$ (i.e. 5 at. % of solute on the liquidus curves) the freezing ranges in the systems Fe–Co, Fe–Cr and Fe–V are about 1·5, 2 and 3° C respectively, and are thus so small that, in spite of the precautions taken, the accuracy of the data is not sufficient to justify the use of Van't Hoff's equation. For the remaining elements the results shown in table 1 are obtained.

TABLE 1

system	calculated value of L (kcal/mole)
Fe–Ti	3·2
Fe–Mn	3·9
Fe–Ni	3·2
Fe–Cu	2·9
experimental value	3·67

The agreement between the calculated and experimental values is as good as can be expected in view of the extreme sensitivity of the calculated L values to small errors in the temperature measurements. Thus an error of 2° C in the solidus points for the two alloys of lowest solute content may affect the calculated value of L by 100 %. We may therefore reasonably conclude that, in marked contrast with the previously accepted data, the present results at infinite dilutions are in good agreement with those expected for monatomic solid and liquid solutions.

For pure Mn, heat-content measurements have not been carried beyond 1200° C (Sully 1955), and the value (3·5 kcal/g atom) for the latent heat of fusion was deduced from vapour-pressure measurements (Kelley 1934; Kubachewski & Evans 1951). In the present work, the freezing ranges for the δ-Mn phases in the systems Mn–V and Mn–Cr are too

* It should be noted that some published data for latent heats of fusion are obtained by the use of Van't Hoff's equation.

PHILOSOPHICAL TRANSACTIONS OF THE ROYAL SOCIETY A MATHEMATICAL, PHYSICAL & ENGINEERING SCIENCES

narrow to justify calculations of L by means of Van't Hoff's equation, but for the remaining systems, the results shown in table 2 are obtained.

These values are of the same order as that deduced from the vapour-pressure data, and confirm that, within the experimental error, the solid and liquid solutions are monatomic. As explained on p. 425 the solidus points were taken to be those of the second arrest point on the heating curve, which was preceded by an arrest at a temperature of 2 to 3° C lower. Quite inconsistent results were obtained for the calculated latent heat of fusion if attempts were made to identify the lower arrest points with the solidus curve, and to join this to the freezing-point of pure Mn.

TABLE 2

system	calculated value of L (kcal/g atom)
Mn–Ti	4·6
Mn–Fe	5·0
Mn–Co	2·2
Mn–Ni	2·8
Mn–Cu	3·2

(v) *Further examination of the δ/γ/liquid equilibrium*

The Van't Hoff equation in the form of § (iv) is the extrapolation to infinite dilution of the more general equation for dilute solutions:

$$(1-x_l)/(1-x_s) = -\Delta G/RT,$$

where x_l and x_s are the atomic fractions of solute in the liquid and solid phases in equilibrium with one another at temperature T, and ΔG is the difference between the free energies of pure liquid, and pure solid Fe at the same temperature. The tables of Darken (1951) referred to above give the melting-point of δ-Fe as 1539° C, at which temperature $\Delta G = 0$. For comparison with the present results it is thus necessary to apply a correction* of 6° C, so as to refer to a melting-point of 1533° C, and when this is done, the straight line in figure 35 shows the relation between ΔG and T. The work of Kubachewski (1949), using the method of equilibrium between water vapour, hydrogen and alloys of different compositions, has shown that at lower temperatures (700 to 900° C) the solid solutions in the system Fe–Ni are practically ideal. Figure 35 shows the values of ΔG calculated from the δ-liquidus and solidus curves, and the agreement is as good as could be expected. The ΔG values calculated from the liquidus and solidus curves of the system Fe–Cu and Fe–Mn are also in good agreement with Darken's values, and for the system Fe–Ti the agreement is good in the very dilute region. For the systems Fe–Co, Fe–Cr and Fe–V the freezing ranges are too narrow for the calculated values to be significant. For the equation to agree with Darken's values, the freezing ranges in these systems would have to be about one-half of those observed, but as the differences are of the order 1 to 3° C we cannot regard them as lying outside the experimental error.

The data of Darken (1951) also enable the values of ΔG to be obtained for the difference between the free energies of liquid iron and solid γ-Fe at temperatures down to 1200° C. These may be compared with the values calculated from the above equation, and the

* Of this difference less than about one-half is due to the impurities in the 'H' iron, and the remainder to the fact that the value 1539° C is based on the old temperature scale.

results are shown in table 17. In the system Fe–Co, the freezing range is again too small to justify calculation. In the system Fe–Ni, the calculated ΔG values at the peritectic temperature, and at 1495° C (the lowest temperature to which the present work was carried), are in reasonable agreement with those of Darken's tables; the freezing range is narrow and the calculated values are very sensitive to small errors in the experimental

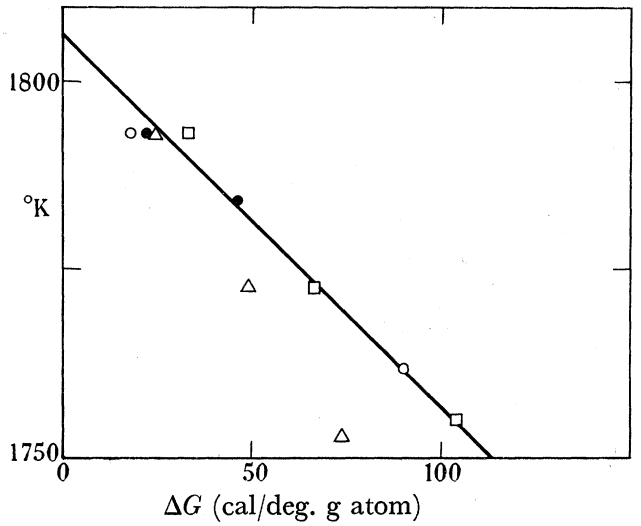

FIGURE 35. Plot of ΔG against temperature from liquidus and solidus slopes in iron-rich alloys: △, Ti; □, Mn; ●, Ni; ○, Cu.

TABLE 3

system	temperature (° C)	calculated value of ΔG for liquid γ–Fe	value of ΔG estimated from Darken's tables
Fe–Ni	peritectic	39	36
	1495	91	71
Fe–Mn	peritectic	108	105
	1450	206	173
	1400	250	252
	1350	348	342
	1300	512	458

work. In the system Fe–Mn, the calculations can be extended to much lower temperatures, and as shown in table 3 there is good agreement between the calculated values of ΔG and those given by Darken. The comparison has been made on the assumption that the temperature adjustment of 6° C referred to previously (p. 450) applies throughout. The data of Darken (when adjusted by 6° C) make the free energies of γ- and liquid Fe to be equal at about 1525° C, whereas the present liquidus and solidus curves extrapolate better to a value of 1520° C or slightly lower. It is felt, however, that the data are not sufficiently precise to justify further corrections. For the system Fe–Cu in which the γ-solidus curve is vertical, the calculated ΔG values are quite different from those of Darken, and the γ-liquid equilibrium is clearly of a different nature.

The above equation also enables us to calculate the width of the two-phase $(\delta+\gamma)$ fields at the peritectic temperatures. The results of these calculations are shown in table 4 and are of the same order as the experimentally determined values. If the results of the preceding calculations for the liquid $\rightleftharpoons$ γ-solid equilibrium are regarded as establishing

the validity of the equation, the results shown in table 4 suggest that, at the higher temperatures, the temperature hysteresis of the transformations was relatively slight, and that the 2-phase fields in the solid state are generally very narrow.

TABLE 4. WIDTH OF TWO-PHASE FIELDS IN IRON AND MANGANESE ALLOYS

system	temperature (° C)		calculated width of two-phase region (at. %) $(\beta+\gamma)$	$(\gamma+\delta)$
Fe–Mn	peritectic	1473	—	0·3
Fe–Co		1500	—	0·4
Fe–Ni		1510	—	0·43
Fe–Cu		1478	—	0·32
Mn–Ti	eutectoid	1121	0·48	0·17
Mn–V	peritectoid	1107	0·24	0·36
Mn–Cr		1110	0·29	0·31
Mn–Fe	peritectic	1133	—	1·23
Mn–Co	peritectoid	1145	0·9	0·13
Mn–Ni	peritectic	1162	—	0·33
Mn–Cu		1098	—	0·48

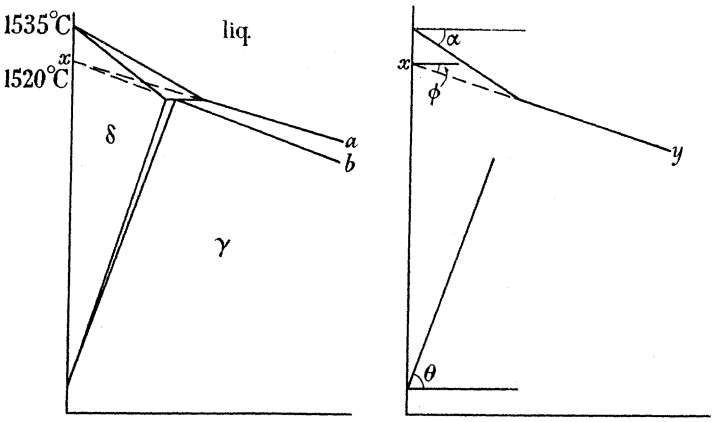

FIGURE 36. Form of phase diagram at γ/δ peritectic.

(vi) *The γ/δ/liquid equilibrium*

The data discussed on p. 451 suggest that if the A_4 transformation did not occur, pure solid γ-Fe would be in equilibrium with pure liquid Fe at about 1520° C. We may, therefore, regard the γ- and δ-solidus and liquidus curves as based on a diagram of the type of figure 36.* In the alloys with Ti, V and Cr, the depression of the curves *xa* and *xb* are to be regarded as greater than those of the corresponding curves for the δ-solid solutions, so that the γ-phase never comes into equilibrium with the liquid.

In figure 36 the phase boundaries refer to the $\delta \rightleftharpoons$ liquid and $\gamma \rightleftharpoons$ liquid equilibria, and since these involve the δ- and γ-phases, we may expect some relation between the slopes of the liquidus and solidus curves, and those of the A_4 transformation curves which refer to the $\gamma \rightleftharpoons \delta$ equilibrium. If the angles α, θ and ϕ are defined as shown in figure 36, the data indicate that for a given value of α an increase in θ (i.e. an increase in the γ-stabilizing power of the solute) produces a decrease in ϕ and more pronounced change of slope at the peritectic horizontal.

* This diagram is of interest in suggesting that with supercooling, alloys of the δ-type may solidify directly to the γ-phase.

Appendix A. Results of thermal analyses

In the following tables the first column shows the atomic percentage of solute.

The second column indicates the transformations to which the arrest temperatures refer, with the following abbreviations: L, liquidus; S, solidus; E, eutectic or eutectoid; P, peritectic.

The third and fourth columns show the arrests obtained from cooling curves and heating curves respectively. The use of brackets implies that the exact value was uncertain owing to supercooling or other causes.

The fifth column includes notes on refractories and other points.

Table A1. Iron–titanium

composition (at. % Ti)	arrest	cooling (° C)	heating (° C)	notes
0·11	L	1531·5	—	alumina re-
	S	—	1528·5	fractories
	γ/δ	1374	1376	were used
	α/γ	910	924	for the first
0·36	L	1529	—	15 alloys
	S	—	1521·5	
	γ/δ	1336	1350	
	α/γ	930	960	
0·63	L	1526	—	
	S	—	1513	
	α/γ	960	(1136)	
1·28	L	1519	—	
	S	—	1498	
	α/γ	(not detected)		
4·27	L	1478	—	
	S	—	1417	
7·1	L	1443	—	
	S	—	1360	
*7·76	L	1430	—	
	S	—	1335	
11·2	L	1379	—	
	E	1288	1287	
15·60	L	1305	—	
	E	1289	1289	
16·06	L	1292	—	
	E	1289	1289	
19·05	L	1335·5	—	
	E	1289	1289	
22·8	L	1370	—	
	E	1289	1289	
27·9	L	1412	—	
	E	1291	1290	
31·1	L	1424	—	
	E	1289	1289	
32·9	L	1427	—	
42·1	L	1407	—	thoria or
	P	1316	1316	thoria-lined
48·3	L	1352	—	refractories
	P	1317	1317	were used
50·9	L	1318	—	for the last
	P	—	1317	4 alloys
53·1	L	1315	—	

Table A2. Iron–vanadium

composition (at. % V)	arrest	cooling (° C)	heating (° C)	tungsten content (at. %)
0·54	L	1531	—	—
	S	—	1530	—
	γ/δ	1345	1360	—
	α/γ	936	965	—
†1·55	L	1530	—	—
	S	—	1527	—
10·1	L	1510	—	0·05
	S	—	1503·5	—
10·5	L	1509	—	0·2
	S	—	1503·5	—
18·5	L	1490·5	—	—
	S	—	1484	—
25·8	L	1478	—	—
17·3	L	1475	—	—
30·5	L	1473·5	—	—
39·4	L	1475	—	0·4

Table A3. Iron–chromium

composition (at. % Cr)	arrest	cooling (° C)	heating (° C)
1·89	L	1530·5	—
	S	—	1528
4·4	L	1527	—
	S	—	1523·5
8·72	L	1521·5	—
	S	—	1517
14·35	L	1514	—
	S	—	1511·5
19·69	L	1510·5	—
	S	—	1510
24·89	L	1512	—
	S	—	1510·5
33·05	L	1520·5	—
	S	—	1516
34·95	L	1524·5	—
	S	—	1518·5
39·8	L	1537·5	—
	S	—	1527

* Analysis of alloy by vacuum fusion methods O = 0·009%; N = 0·015%.
† Analysis of alloy by vacuum fusion methods O = 0·014%; N = 0·008%.

TABLE A4. IRON–MANGANESE

composition (at. % Mn)	arrest	cooling (° C)	heating (° C)
1·9	L	1522·5	—
	S	—	1514
4·64	L	1510	—
	S	—	1499
	γ/δ	1444	1446
6·94	L	1499	—
	S	—	1487
	γ/δ	1458·5	1459·5
*8·64	L	1491	—
	S	—	1478
	γ/δ	(1466)	1468
10·09	L	1484·5	—
	S	—	1470
	γ/δ P	(1470)	1473
11·87	L	1480·5	—
	S	—	1466
	γ/δ P	(1465)	1473·5
13·8	L	1469·5	—
	S	—	1451
23·4	L	1440	—
	S	—	1421·5

TABLE A5. IRON–COBALT

(After Harris & Hume-Rothery 1953)

composition (at. % Co)	arrest	cooling (° C)	heating (° C)
0	L	1534	—
	γ/δ	1388	1391
2·98	L	1528	—
	S	—	1525
	γ/δ	1412	1411·5
6·12	L	1522·5	—
	S	—	1517·5
	γ/δ	1428	1431
8·54	L	1518	—
	S	—	1515
	γ/δ	1448	1449
10·46	L	1516	—
	S	—	1512
	γ/δ	1459	1460
12·46	L	1511·5	—
	S	—	1508·5
14·02	S	—	1502
	γ/δ	—	1478
16·47	L	1503	—
	S	—	1499·5
	γ/δ	1489	1490
16·99	L	1500·5	—
	S	—	1498·5
19·23	L	1500	—
	S	—	1489
22·51	L	1497	—
	S	—	1494
24·5	L	1495	—
	S	—	1492
28·83	L	1491	—
	S	—	1489·5
31·27	L	1488	—
	S	—	1486

TABLE A6. IRON–NICKEL†

composition (at. % Ni)	arrests	cooling (° C)	heating (° C)
1·84	L	1524	—
	S	—	1522
	γ/δ	1451	1458
2·79	L	1520	—
	S	—	1516
	γ/δ	1480	1479
3·76	L	1517	—
	S	—	1511
	γ/δ	1500	1503·5
‡4·62	L	1513	—
	S	—	1508·5
	P	1511	—
5·27	L	1510·5	—
	S	—	1507
7·61	L	1506·5	—
	S	—	1501·5
8·95	L	1500·5	—
	S	—	1496·5
12·33	L	1495	—
	S	—	1489

† Some of these results were obtained by the late Mr. G. B. Harris.

TABLE A7. IRON–COPPER

composition (at. % Cu)	arrest	cooling (° C)	heating (° C)
‖2·60	L	1516	—
	S	—	1510
4·81	L	1503	—
	S	—	1493
	γ/δ	1461·5	1462
6·67	L	1496	—
	γ/δ	1473	1472
7·44	L	1490·5	—
	γ/δ	1474	1475
8·98	L	1484	—
	P	1476·5	1478
9·17	L	1484	—
	P	1478	(1481)
9·8	L	1478	—
13·3	L	1472	—
19·68	L	1455	—
28·6	L	1438	—
	α/γ peritectic	1088	1088

Analyses of alloys by vacuum fusion methods:

* O = 0·008%.
‡ O = 0·01%; N = 0·005%.
‖ O = 0·015%; N = 0·005%.

PHILOSOPHICAL TRANSACTIONS OF THE ROYAL SOCIETY A MATHEMATICAL, PHYSICAL & ENGINEERING SCIENCES

TABLE A8. MANGANESE–TITANIUM

composition (at. % Ti)	arrest	cooling (° C)	heating (° C)
0·14	δ/γ	1131	1132
	β/γ	1099	1100
0·38	L	1244	—
	S	—	1243
	γ/δ	1124	1124
	β/γ	1110	1117
0·97	L	1241	—
	S	—	1238·5
	β	1125	1126·5
2·38	L	1236	—
	S	—	1233
	β/δ	1141	1141
3·12	L	1231	—
	S	—	1226
	δ/Mn_3Ti	1155·5	—
4·29	L	1228	—
	δ/Mn_3Ti	1166	—
5·10	L	1223	—
	S	—	1216
	δ/Mn_3Ti	1177	—
7·14	L	1216	—
	S	—	1207
	δ/Mn_3Ti	1200	—
7·8	L	1211	—
	E	1204	1204
9·4	E	1204	1203·5
9·5	L	1208	—
	E	1204	1204
12·3	L	1220	—
	E	1204	1203·5
15·0	L	—	1235
	P	1229	—
	E	1204	1204
16·6	L	1255	—
	P	1226	—
18·6	L	1269	—
	P	1248·5	—
	P	1230	1231
	E	1202	1202
22·0	L	1292	—
	P	1248·5	1255
	P	1230	1234
	E	1200	—
25·3	L	1305	—
	P	1248	1255
	P	1230	1234
29·7	L	1317	—
	P	1246	1251
	P	1228	—
(33·9)	L	1324	—*
(41·3)	L	1318·5	—*
(46·4)	L	1300	—*
	E	1181	1181*
(51·2)	L	1272	—*
	E	1181	1181*

* thoria.

TABLE A9. MANGANESE–VANADIUM

composition (at. % V)	arrest	cooling (° C)	heating (° C)
0·42	L	1246·5	—
	S	—	1245
	γ/δ	1118	1118
	β/γ	1102	1102
0·97	L	1249	—
	S	—	1246·5
	β/δ	1102·5	1105·5
2·98	L	1260	—
	—	—	1255
	β	1079	1083
5·95	L	1279	—
	S	—	1267
	β/δ	1042	—
7·74	L	1294	—
	S	—	1275
	E	1009	1027
9·62	L	1313	—
	S	—	1285
	E	1013	1027
15·04	L	1362	—
	S	—	1315
	σ/δ	1026	1039

TABLE A10. MANGANESE–CHROMIUM

composition (at. % Cr)	arrest	cooling (° C)	heating (° C)
0·48	L	1245	—
	S	—	1244
	γ/δ	1118·5	1120·5
	β/γ	1101	1104·5
0·96	L	1245·5	—
	S	—	1244·5
	β/δ	1108	1110
3·22	L	1248·5	—
	S	—	1247
	β/δ	1093·5	1095·5
6·98	L	1258	—
	S	—	1255
	β/δ	(1069)	1065
8·09	L	1261·5	—
	S	—	1258
	β/δ	1054	1039
9·31	L	1267	—
	S	—	1261
	β/δ	1029	1014
10·6	L	1273	—
	S	—	1266
	E	992	1010
11·65	L	1278	—
14·78	L	1292	—

PHILOSOPHICAL TRANSACTIONS OF THE ROYAL SOCIETY A MATHEMATICAL, PHYSICAL & ENGINEERING SCIENCES

TABLE A11. MANGANESE–IRON

composition (at. % Fe)	arrest	cooling (° C)	heating (° C)
0·9	L	1241	—
	S	—	1237
	γ/δ	1137·5	1138
	β/γ	1095	1096·5
2·72	L	1237	—
	S	—	1234
	γ/δ	1158·5	1156·5
	β/γ	1109	1107·5
4·86	L	1236	—
	S	—	1233
	δ/γ	1173	1175·5
	β/γ	1121·5	1125
10·23	L	1234	—
	S	—	1233
	γ/δ	1207·5	1211·5
	β/γ	1148·5	1152
11·01	L	1233	—
	S	—	1231
	γ/δ	1216·5	1221
	β/γ	1148·5	1154
13·09	L	1233·5	—
	S	—	1232
	β/γ	1153·5	1157
17·25	L	1240	—
	S	—	1237
	β/γ	1148	1151
19·93	L	1246·5	—
	S	—	1241
	β/γ	1145·5	1140
24·7	L	1258	—
	S	—	1249
	β/γ	1127	—
32·2	L	1290	—
	S	—	1275
44·3	L	1313	—
	S	—	1288
50·09	L	1340	—
	S	—	1316
64·5	L	1392	—
	S	—	1375
68·14	L	1406	—

TABLE A12. MANGANESE–COBALT

composition (at. % Co)	arrest	cooling (° C)	heating (° C)
1·04	L	1237·5	—
	S	—	1235
	γ/δ	1137·5	1140
	β/γ	1102·5	1105·5
3·86	L	1222	—
	S	—	1216
	γ/δ	1245	1245
	β/γ	1237	1240
4·85	L	1216	—
	S	—	1210
	β/δ	1151	1151
7·84	L	1201·5	—
	S	—	1189
	β/δ	1173	1168
9·27	L	1193	—
	S	—	1182
	β/δ	1181	1178
10·2	L	1187·5	—
	S	—	1180
	P	1182·5	—
13·75	L	1180·5	—
	S	—	1178
16·2	L	1177	—
	S	—	1175
19·6	L	1174	—
	S	—	1172
24·8	L	1169	—
	S	—	1168
29·7	L	1166	—
	S	—	1165
36·36	L	1160·5	—
	S	—	1160·5
38·1	L	1161	—
	S	—	1160
	β Mn/β Co	1150	—
41·7	L	1167	—
	S	—	1160
43·56	L	1173	—
	S	—	1163
46·1	L	1181	—
	S	—	1170

PHILOSOPHICAL TRANSACTIONS OF THE ROYAL SOCIETY A MATHEMATICAL, PHYSICAL & ENGINEERING SCIENCES

TABLE A13. MANGANESE–NICKEL

composition (at. % Ni)	arrest	cooling (° C)	heating (° C)
0·95	L	1235	—
	S	—	1226·5
	γ/δ	1141	1141
	β/γ	1075	1078
3·66	L	1212	—
	S	—	1189
	γ/δ	1154	1154
	β/γ	1036	1044
5·85	L	1193	—
	P	1162	1162
6·31	L	1188	—
	P	1161	1163
8·99	L	1165	—
	S	—	1135
	P	1161	—
10·45	L	1155	—
	S	—	1126

TABLE A14. MANGANESE–COPPER

composition (at. % Cu)	arrest	cooling (° C)	heating (° C)
0·86	L	1237	—
	S	—	1229
	γ/δ	1134·5	1134·5
	β/γ	1022	1041
1·9	L	1230	—
	S	—	1220
	γ/δ	1133	1133
5·1	L	1210	—
	S	—	1182
	γ/δ	1125	1125
8·7	L	1185	—
	S	—	1134
	γ/δ	1110	1109
11·15	L	1170	—
	S	—	1116
	γ/δ	1102	1100
12·06	L	1165	—
	γ/δ	1097	1101
13·43	L	1159	—
	γ/δ	1096	1098·5
19·31	L	1124	—
	γ/δ	1093·5	1100
28·4	L	1072	—

APPENDIX B. CHEMICAL ANALYSES

The authors are indebted to Mr K. Speight and associates, of the B.I.S.R.A. laboratories at Sheffield, for chemical analysis of alloys.

Whole ingots or half ingots were dissolved for chemical analysis, errors due to segregation thus being avoided. Each ingot or half ingot was examined spectrographically by means of a d.c. arc technique, and where a significant impurity was recorded this was analyzed chemically.

The sample was weighed as a single piece and then subjected to a suitable acid treatment to achieve solution. The insoluble residue was filtered off and weighed and this weight deducted from that of the original ingot. All subsequent calculations were based upon the adjusted sample weight.

Spectrographic examination of the insoluble residue was undertaken occasionally. This was found to consist of alumina and the oxidized outer skin present on the ingot prior to solution. As a check on the results obtained for the alloying constituent, occasional analyses were carried out to determine the remainder.

Wherever British Standard methods existed, these were adopted. In the absence of British Standards, recognized recommended methods were employed.

The reproducibility of results depended partly upon the element in question and partly upon the composition of the alloy.

The following are estimates of the reproducibility given by Mr Speight for the elements concerned:

Titanium	
Less than 4 % Ti	±0·03 %
More than 4 % Ti	±0·2 %
Vanadium	
Less than 1 % V	±0·015 %
With 40 % V	±0·25 %
Chromium	
With 1 % Cr present	±0·02 %
5 %	±0·05 %
25 %	±0·1 %
Manganese	
With 1 % Mn present	±0·03 %
14 %	±0·1 %
25 %	±0·15 %
Iron	
Less than 5 % Fe	±0·05 %
With 50 % Fe present	±0·15 %
Cobalt	
According to Co content	± 0·02 to ±0·15 %
Nickel	
With 1·0 % Ni present	±0·01 %
15 %	± 0·1 %
Copper	
With 15 % Cu present	±0·1 %

The authors must express their gratitude to Professor Sir Cyril Hinshelwood, P.R.S., to Dr F. M. Brewer for laboratory accommodation and other facilities which have greatly encouraged the present research. Thanks are due to the British Iron and Steel Research Association which has provided a research bursary for one of the authors (A.H.), and has made grants towards the cost of refractories, and has also undertaken the chemical analyses, in connexion with which the authors must express their extreme indebtedness to Mr K. Speight for his care and attention. The Council of the Royal Society must also be thanked for financial assistance towards the expenses of the research.

PHILOSOPHICAL TRANSACTIONS OF THE ROYAL SOCIETY A MATHEMATICAL, PHYSICAL & ENGINEERING SCIENCES

References

Adcock, F. 1931 *J. Iron Steel Inst.* **124**, 99.

Adcock, F. 1937 *J. Iron Steel Inst.* **135**, 288.

Andrews, K. W. 1952 *Metal Treatm.* **19**, 425, 489.

Basinski, Z. S. & Christian, J. W. 1954 *Proc. Roy. Soc.* A, **223**, 554.

Bristowe, C. A. 1939 *Spec. Rep. Iron St. Inst., Lond.*, **24**, 1.

Carlile, S. J., Christian, J. W. & Hume-Rothery, W. 1949 *J. Inst. Met.* **76**, 169.

Coles, B. R. & Hume-Rothery, W. 1951 *J. Inst. Met.* **80**, 85.

Darken, L. S. & Smith, R. P. 1951 *Industr. Engng Chem.* **43**, 1815.

Gayler, M. L. V. 1933 *J. Iron Steel Inst.* **128**, 293.

Hansen, M., McPherson, D. J. & Rostoker, W. 1953 *Wright Air Development Centre Rep.* no. 41.

Harris, G. B. & Hume-Rothery, W. 1953 *J. Iron Steel Inst.* **174**, 212.

Hildebrand, J. & Scott, R. L. 1950 *Solubility of non-electrolytes.* New York: Reinhold Publishing Corporation.

Hume-Rothery, W. & Raynor, G. V. 1954 *The structure of metals and alloys.* London: Inst. of Metals.

Kelley, K. K. 1935 *Contributions to the data on theoretical metallurgy.* U.S. Bureau of Mines.

Kubachewski, O. & Evans, E. Ll. 1951 *Metallurgical thermochemistry.* London: Butterworth-Springer Ltd.

Kubachewski, O. & von Goldbeck, O. 1949 *Trans. Faraday Soc.* **45**, 948.

Maddocks, W. R. & Clausen, G. E. 1936 *Spec. Rep. Iron St. Inst., Lond.*, **14**, 97.

Pearson, W. B. & Christian, J. W. 1951 *Nature, Lond.*, **167**, 110.

Potter, E. V. & Lukens, H. C. 1947 *Trans. Amer. Inst. Min.* (*Metall.*) *Engrs*, **171**, 401.

Ruer, R. 1927 *Z. anorg. Chem.* **164**, 366.

Schubert, A. 1955 *Arch. Eisenhüttenw.* **26**, 299.

Smithells, C. J. 1955 *Metals reference book.* London: Butterworths Scientific Publications.

Sully, A. H. 1955 *Manganese.* London: Butterworths Scientific Publications.

Sutton, A. L. & Hume-Rothery, W. 1955 *Phil. Mag.* **46**, 1295.

Wever, F. 1929 *Arch. Eisenhüttenw.* **2**, 739.

Witte, H. & Wallbaum, H. J. 1938 *Z. Metallk.* **30**, 100.

Zwicker, V. 1949 *Z. Metallk.* **42**, 277.

PHILOSOPHICAL TRANSACTIONS OF THE ROYAL SOCIETY A MATHEMATICAL, PHYSICAL & ENGINEERING SCIENCES